Bachelor’s Thesis

Evaluation of Spatial Distribution of Creep Void in Heat-Affected Zone of Modified 9Cr-1Mo Steel

p.1~p.62

Submitted on February 3rd, 2012

Under the supervision of Associate Professor Satoshi Izumi

100176 Watcharaphon Uttranuson

Foreword

As power plants nowadays tend to push their efficiency to the extremely high level, innumerable new materials have been introduced regularly. One of the recent materials applied to high-pressured steam tubes is modified 9Cr-1Mo steel, commonly used in so-called Ultra Super Critical Power Plant. Modified 9Cr-1Mo steel is known to have superior high temperature strength. There have been, however, several reports regarding problems related to type IV cracking and creep damage taking place in the heat affected zone or the weld joints of the material. To identify the area where creep damage occurred and reveal the cause, we approached the problem in two methods. First, we observed the surface of the heat-affected zone of a cross-section of a weld-joint part of material from Central Research Institute of Electric Power Industry with scanning electron microscope. The data helps us define the area where creep voids and creep damage mainly take place and further out understanding of disputable creep void mechanics. In addition, Vicker's hardness distribution and grain size distribution were measured; further definition and characteristics of creep damage phenomenon area can be discovered. The other approach concerns finite element analysis method (FEM) of the tube with longitudinal welding. The result of stress distribution and creep strain distribution in material helps explain the characteristic of void distribution and void area distribution.

Contents

List of Items

Chapter 1: Introduction

1.1 Background

Recently, the revolution of renewable energy has invoked orthodox coal-fired power plants into pursuing even higher efficiency (electric generation efficiency 42%)[1] while staying with the same or even lower CO_2 emission. This resulted in so-called Ultra Super Critical Power Plant, which pushes power generating conditions to the extreme. Data taken in 2008 showed that coal-fired USC power plants made up over 27% of the power plants in Japan. In general, USC power plants work with extremely high temperature (600℃ or higher), extremely high pressure (21.7MPa or higher), and long continuous operating time (approximately 20,000 hours)[2]. The pros and cons of USC power plants are listed below:

<u>Pros</u>	<u>Cons</u>
1. High thermal efficiency	1. Materials limitation
2. Low CO_2 emission (fig. 1.1a)	2. High level of corrosion
3. Low fuel cost per unit	3. High maintenance cost
4. Raw coal can be directly used	

Due to the pros and cons above, USC power plants received a lot of attention and thought to be the first choice for energy investment world-wide scale in the next decade to come. (fig. 1.1c) Especially for Japan who has surpassed Italy and United Kingdom in respect of thermal efficiency (from fig.1.1b) and confronted serious energy crisis after the discontinue of nuclear power plants due to the meltdown incident in Fukushima, USC power plants become the sole answer at the moment.

However, high level of corrosion mentioned above includes creep rupture. High temperature and high pressure are considered the fundamental condition that induces creep rupture in the material. Widely used material for steam tube is modified 9Cr-1Mo steel for its superior high temperature strength.

Despite its proud strength in high temperature condition, there are reports of accidents occurred at the weldment of the steam tube such as the one in fig. 1.1d. The cause of the accidents was considered to be type IV crack taking place at the fine-grained area of the welding's heat affected zone[1],[3]. This study focuses on the surface of the cross-section of steam tube, exclusively at the heat affected area. Mechanisms of Type-IV failure, however, have not been fully understood by preceding researches in respect of its origin. The previous studies on the area either covered only specific points of the surface of heat affected zone, not distribution of every point, or showed the relation of creep void distribution and creep strain but not included data of hardness distribution or void grain size distribution[3]. The wider scope of number of data and types of data would help clarify the disputable characteristic of creep void spatial distribution.

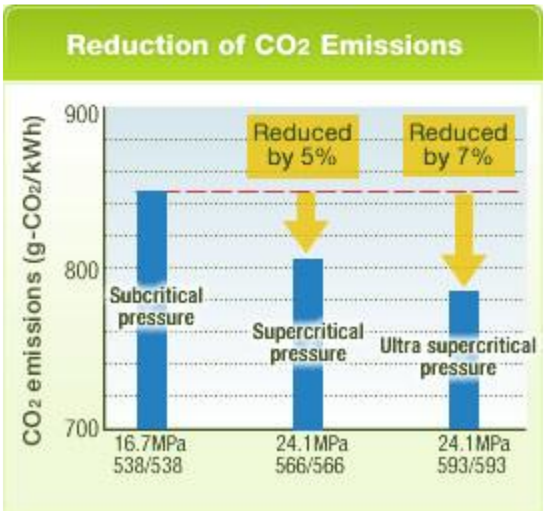

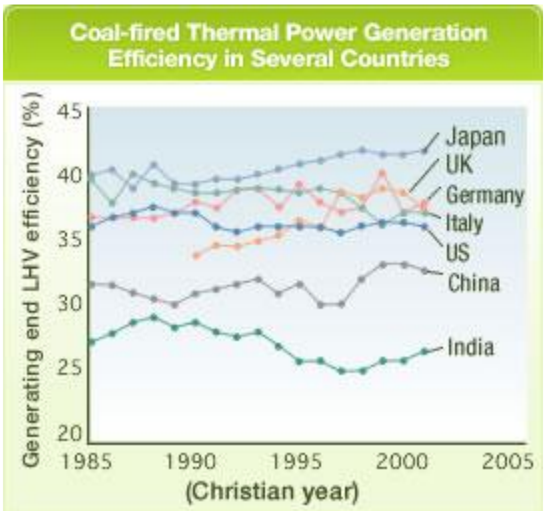

↑ (Left)Fig. 1.1a reduction of CO2 Emissions by USC plants[4]

↑ (Right) Fig. 1.1b Global data on power generating efficiency[5]

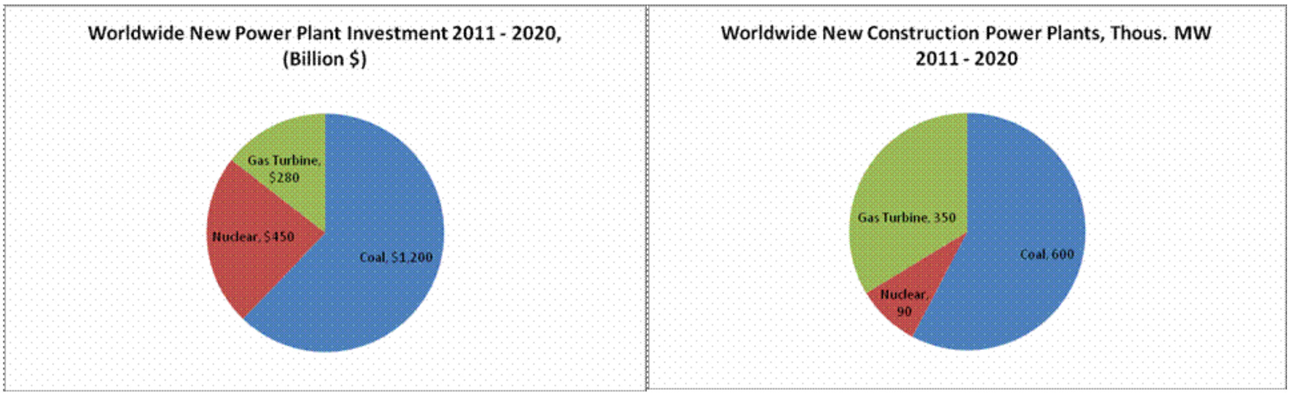

↑ Fig. 1.1c Year 2011-2020 USC power plants trend [6]

↑ Fig.1.1d Failure by a loss of creep-rupture strength [7]

1.2 Objective

This study focuses on unveiling the relation of the distribution of void distribution, void surface distribution, grain size, Vicker's hardness, the distribution of stress, the distribution of creep strain, and triaxiality factor by FEM analysis using ANSYS simulation.

The question to be answered is where creep damage tends to occur and how. Previous researches mostly concluded that the most crucial factor was triaxiality factor, so this research also includes triaxiality factor as one of the main parameters together with other data.

1.3 Outline of Research

This research is divided into 6 separating chapters.

First chapter includes Introduction, Background, and Outline of this research. This chapter also defines the scope and previous research on the topic. Here we will notify the importance of this research and the merit of the outcome.

Second chapter mainly focuses on the fundamental theories of this research which are triaxiality factor, creep strain theory, and characteristic of interior creep hardness. These basic elements are extremely crucial to conclude the result of observation and simulation.

Third chapter concerns how preparation and measurement had been performed in this research. Since there are many procedures to be thoroughly explained, this chapter is separated into seven sub-chapters. The properties of test specimens are also mentioned here.

Forth chapter shows how the simulation via finite element method has been carried out. The aim of the simulation is to explain the characteristics of creep void we have observed.

Fifth chapter is the compilation and discussion of the results. We will investigate the connection between the result of Third and Forth chapter.

Sixth chapter puts down to the conclusion and future plan for further research concerning this topic.

For more methodical outline details, the research is divided into 4 separated components, consisting of preparation, observation, analysis, and discussion as showed in fig. 1.3.

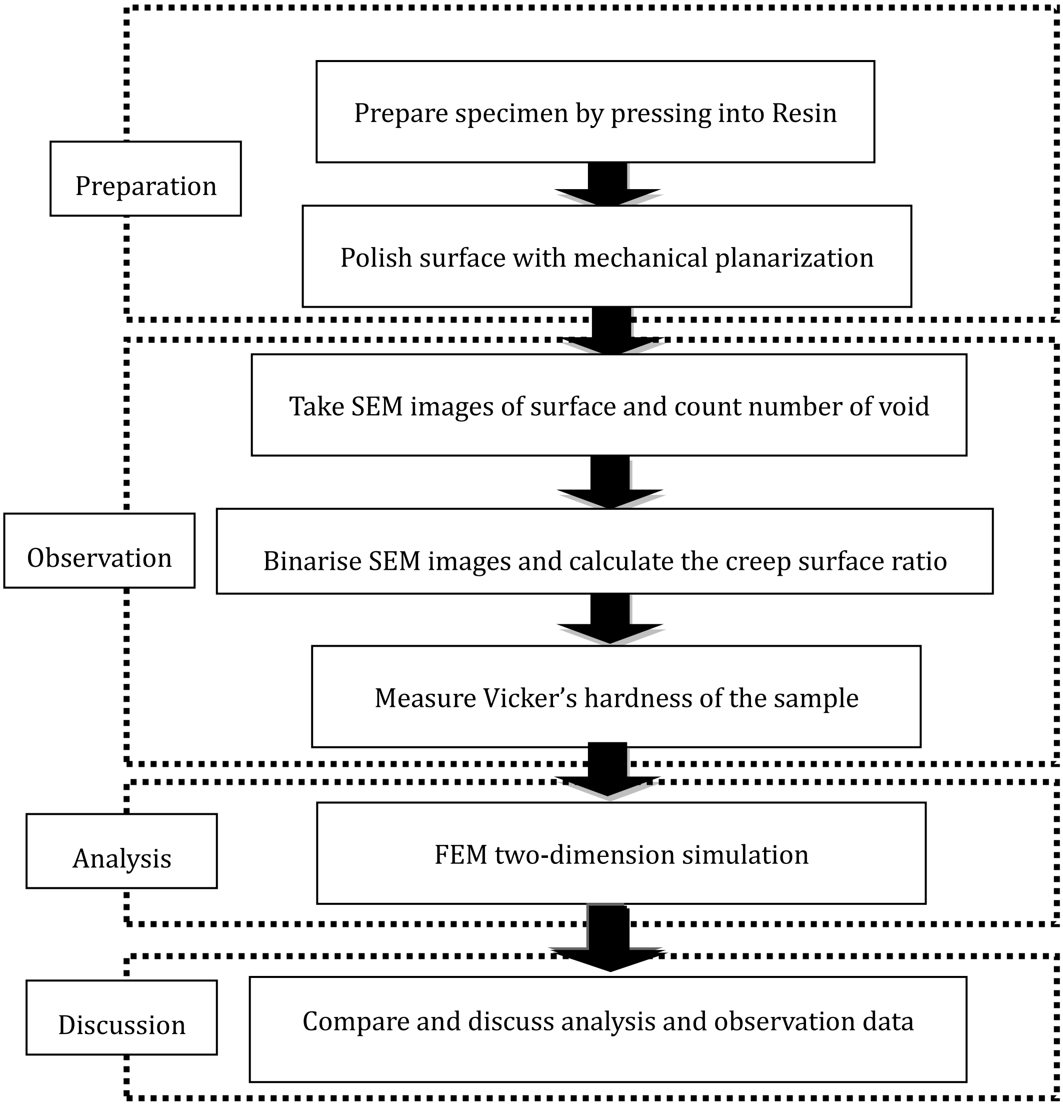

↑ Fig. 1.3 outline of research

Chapter 2: Basic Theory

2.1 Triaxiality Factor

It is known that a triaxiality stress state reduces locally the ductility of materials. We focus in the effect of triaxiality factor on strength of material working at high temperature and high stress. The Triaxiality Factor is defined as,

$$TF = \frac{\sqrt{2}(\sigma_1 + \sigma_2 + \sigma_3)}{\sqrt{(\sigma_1 - \sigma_2)^2 + (\sigma_2 - \sigma_3)^2 + (\sigma_1 - \sigma_3)^2}} = \frac{3\sigma_M}{\sigma_{mises}} \tag{2.1-1}$$

Where, in the above formula,

$\sigma_1, \sigma_2, \sigma_3$ are principal stresses, respectively.[3]

σ_{mises} is von Mises stress.

$$\sigma_{mises} = \sqrt{\frac{(\sigma_1 - \sigma_2)^2 + (\sigma_2 - \sigma_3)^2 + (\sigma_1 - \sigma_3)^2}{2}} \tag{2.1-2}$$

As horizontal stress increases, σ_{mises} also increases resulting in higher TF value. On the contrary, as 3 main-axis stresses approach the same value, σ_{mises} decreases as well as the value of TF. Previous research by Masaaki Tabuchi and Hiromichi Hongo of National Institute for Materials Science, the equivalent creep strain is high near the specimen surfaces, and low from a quarter depths to the center of plate thickness. The TF shows high values in the areas from a quarter depths of thickness to the center of thickness, while it is the smallest in the surface areas. In the experimental results

↓ Table 2.1a Triaxiality Factor Calculation

Normalized Principal Stresses			Calculated TF	Description
σ_1	σ_2	σ_3		
1	0	0	1	Uniaxial Tension

1	1	0	2	Biaxial Tension
1	1	1/4	3	Triaxial Tension
1	1/2	1/2	4	Triaxial Tension
1	1	1/2	5	Triaxial Tension
1	1	1	∞	Triaxial Tension
1	-1	0	0	Tension/Compression
1	-1/2	0	0.378	Tension/Compression
1	1	-1	0.5	Biaxial Tension/Compression
1	-1	-1	-0.5	Tension/Compression/Compression
-1	-1	-1	-∞	Triaxial Compression

The present knowledge of the stress triaxiality factor can affect the rupture generally by two ways. Firstly, it basically prevents the plastic deformation while the level of the stress increases, and eventually the rupture stress is being reached and a rupture crack is obtained. Next mechanism is by producing void growths inside the materials. The preexisting micro void is primary target of this growth. Because of plastic straining, those voids are enlarged in a way that is supported by local triaxiality until those voids merge together or the creep rupture occurs. These double natures of the failure by triaxiality factor make it difficult to justify the relation between stress triaxiality and local ductility reduction. [12]

Creep Strain Speed Characteristic and Norton's Law

$$\dot{\varepsilon}_c = B\sigma^n \qquad (2.1\text{-}3)$$

Where, $\dot{\varepsilon}_c$ is creep strain rate, and

σ is Mises stress.

B and power n are material constants that depend on temperature and stress of creep strain.

2.2 Creep Behavior of Isotropic and Anisotropic materials

Experimental observations and measurements are generally accepted to constitute the backbone of physical sciences and engineering because of the physical insight they offer to the scientist for formulating the theory. The concepts that are developed from observations are used as guides for the design of new experiments, which in turn are used for validation of the theory. Thus, experiments and theory have a hand-in-hand relation. [13]

However, it must be noted, that experimental results can differ greatly from reality just like a bad mathematical model (BETTEN, 1973)

Creep tests are carried out on a specimen loaded, in tension or compression, usually at constant load, inside a furnace which is maintained at a constant temperature T. The extension of the specimen is measured as a function of time. A typical creep curve for metals is present in figure 2.1 below.

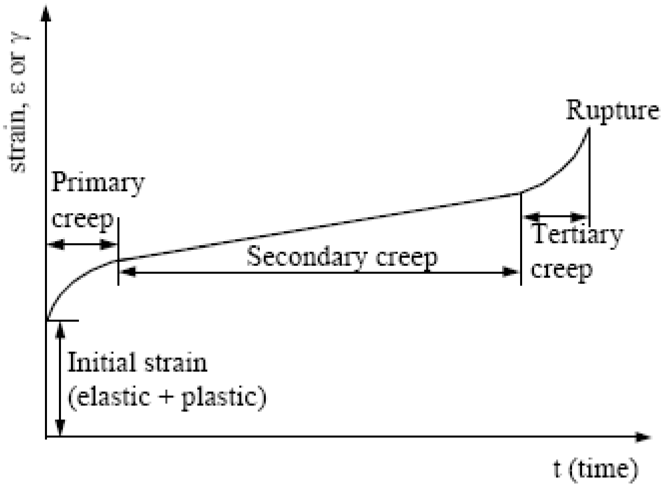

↑ Fig. 2.1 typical creep curve[14]

The temperature at which materials begin to creep depends on their melting point T_M, for instance, $T > 0.4T_M$ for metals and $T > 0.5T_M$ for ceramics.

The response of the specimen loaded by σ_0 at time $t = 0$ can be divided into an elastic and a plastic part as

$$\varepsilon_0 = \frac{\sigma_0}{E(T)} + \varepsilon_p(\sigma_0, T) \qquad (2.2.1)$$

Where *E(T)* is the modulus of Elasticity. The creep strain in fig. 2.1 can then be expressed according to

$$\varepsilon_c = \varepsilon(t) - \varepsilon_0 \propto t^K \qquad (2.2.2)$$

Where $K<1$ in the primary, $K=1$ in the secondary, and $K>1$ in the tertiary creep stage. These terms correspond to a decreasing, constant, and increasing strain rate, respectively, and were introduced by ANDRADE(1910). These three creep stages are often called transient creep, steady creep, and accelerating creep; respectively.

The results (2.2.1) and (2.2.2) from the creep tests justify a classification of material behavior in three disciplines: elasticity, plasticity, and creep mechanics.

Due to proposal of HAUPT(2000), one can also distinguish four theories of material behaviors as follow:

1. The theory of elasticity is concerned with the rate-independent behavior without hysteresis.

2. The theory of plasticity specifies the rate-independent behavior with hysteresis.

3. The theory of viscoelasticity describes the rate-dependent behavior without equilibrium hysteresis.

4. The theory of viscoplasticity is devoted to the rate-dependent behavior with equilibrium hysteresis.

Now, let us discuss the primary, secondary of isotropic and anisotropic materials.

2.2.1 Primary creep

The primary of transient creep is characterized by a monotonic decrease in the rate of creep, and the creep strain can be described by the simple formula

$$\varepsilon_C = A\sigma^n t^m \qquad (2.2.1.1)$$

Where the parameters A, n, m depend on the temperature. They can be determined in a uniaxial creep test. For instance, PANTELAKIS (1983) found in experiments on the austenitic steel X8 Cr Ni Mo Nb 16 16 at 973K the values $A = 3.85\text{x}10^{-15}(\text{N/mm}^2)^{-n}\text{h}^{-m}$, n=5.35 and m=0.22. Further applications of mechanical equations of state were discussed by LUDWIK(1909), LUBAHN and FELGAR(1961), TROOST et al(1973).

If the stress σ in (2.2.1) is assumed to be constant the creep rate $d \approx \dot{\varepsilon}_c$ is given by

$$\dot{\varepsilon}_c = Am\sigma^n t^{m-1} \qquad (2.2.1.2)$$

This relation may be generalized to multiaxial states of stress according to the following tensorial linear constitutive equation.

$$d_{ij} = \frac{3}{2} K(\grave{J}_2)^{(n-1)/2} \grave{\sigma}_{ij} t^{m-1} \qquad (2.2.1.3)$$

,where d_{ij} are the Cartesian components of the rate-of-deformation tensor, and $\grave{J}_2$ is the quadratic invariant of the stress deviator ($\grave{\sigma}_{ij}$).

Substituting the time t from 2.2.1.1 into 2.2.1.2, we arrive at the relation

$$\dot{\varepsilon}_c = mA^{1/m} \sigma^{n/m} \varepsilon_c^{(m-1)/m} \qquad (2.2.1.4)$$

This equation characterizes the strain-hardening-theory. In contrary, strain rate equation (2.2.1.4) contains stress and time as variables. The equation is called the time-hardening-law.

2.2.2 Secondary Creep

Creep deformations of the secondary stage are large and of similar character to plastic deformations. For example, creep deformations of metals will usually be influenced if a hydrostatic pressure is superimposed. Therefore, such creep behavior can be treated with methods of the Mathematical theory of plasticity. The theory of plastic potential (MISES, 1928 :HILL, 1950) can be used in the mechanics of creep. [13]

Chapter 3: Measurement Procedure

3.1 Property of Test Specimen

↓ Table 3.1a test condition and specimen basic property[2]

Material	Modified 9Cr-1Mo Steel
Shape Description	φ60mm×t10mm Oblateness 0.05%
Highest Temperature	571℃
Highest Pressure	21.7MPa
Cumulative Operating Time	6700hours

↓ Table 3.1b chemical components of 9Cr-1Mo Steel[2]

C	**Si**	**Mn**	**P**	**S**	**Cr**	**Mo**	**V**	**Cu**	**Ni**	**Al**	**Nb**	**N**
0.09	**0.26**	**0.44**	**0.014**	**0.001**	**8.29**	**0.88**	**0.2**	**0.001**	**0.006**	**0.01**	**0.06**	**0.045**

↓ Table 3.1c mechanical property of 9Cr-1Mo Steel[2]

Tensile Strength(MPa)	Proof Stress(MPa)	Elongation (%)
681	508	37

The material used in this research is modified 9Cr-1Mo steel of which chemical components are showed in the table 3.1b above and mechanical properties are showed in table 3.1c. Test specimen is created to resemble a part of a steam tube with outer radius of 30mm, thickness of 10mm, and length or 350mm. After welding under condition in table 3.1d below, damage inspection, magnetic particle inspection and radiographic inspection were arranged, and as a result, no defect was found. Next, the eccentricity measurement was performed on the outer surface of the specimen resulting in 0.05%. After welding, material was taken into experiment under condition listed in table 3.1a above. Microstructure and cross-section surface hardness of the specimen is presented below in fig.3.1a. Vicker's hardness of base metal is approximately 225, weld metal is 290. The area of weld metal intimate to the coarse grain area appears to have the highest value. By contrast, a part of the fine-grain area of heat affected zone adjacent to base metal, called 'Intercritical Area', is the most malleable with Vicker's hardness of 211. Heat affected zone is known to be consisted of two major types of elements: first is coarse-grained area which locates next to weld metal area, the other is fine-grained area covering most of the heat affected area. For mod.9Cr steel, the typical grain size for coarse grain is 5-8µm.

↓ Table 3.1d welding condition of specimen[2]

Welding Condition
Welding Method: TIG Welding
Welding Material: TGS − 9Cb
Post heat treatment condition
Temperature: 745°C ± 15°C

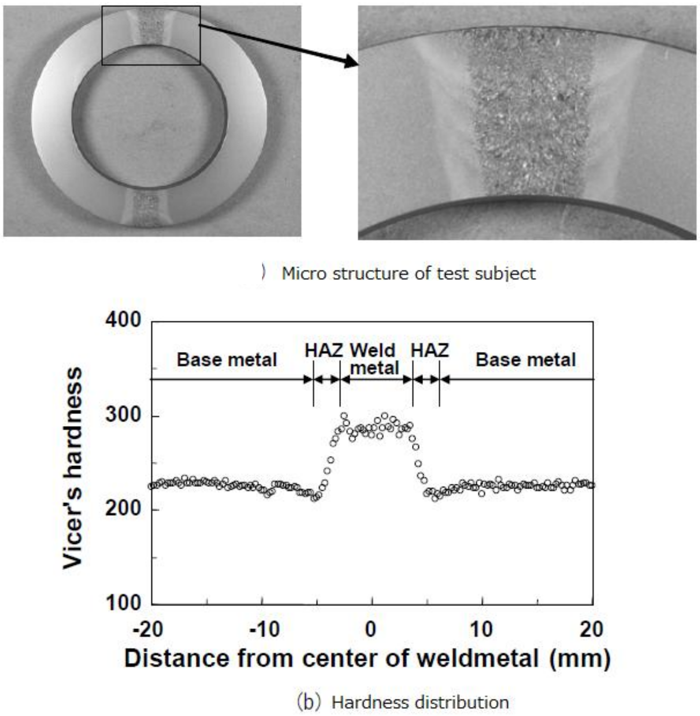

↑ Fig. 3.1a microstructure d hardness distribution of specimen [2]

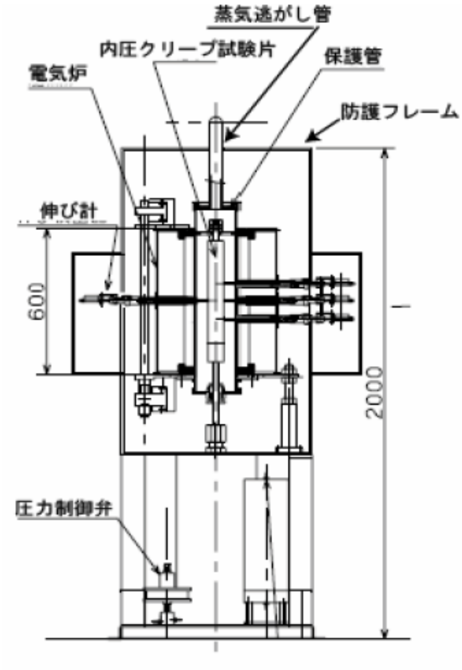

Illustration of a internal pressure creep testing machine.

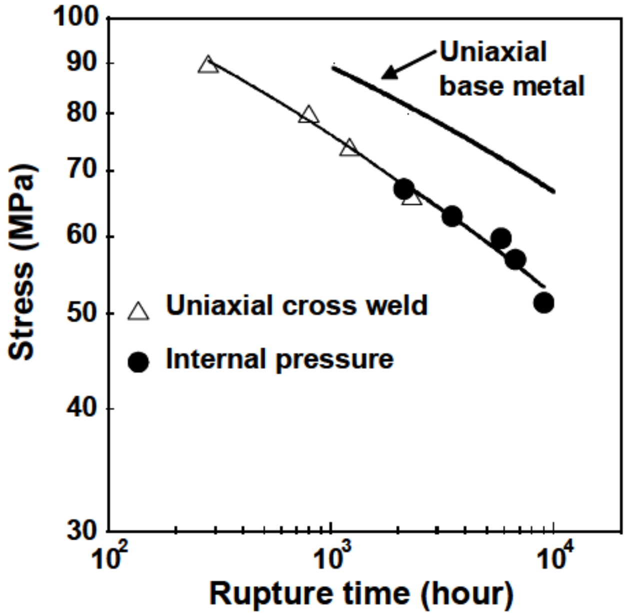

Internal pressure creep test results.

↑ Fig. 3.1b internal pressure creep test machine[2] ↑ Fig. 3.1c internal pressure creep result [2]

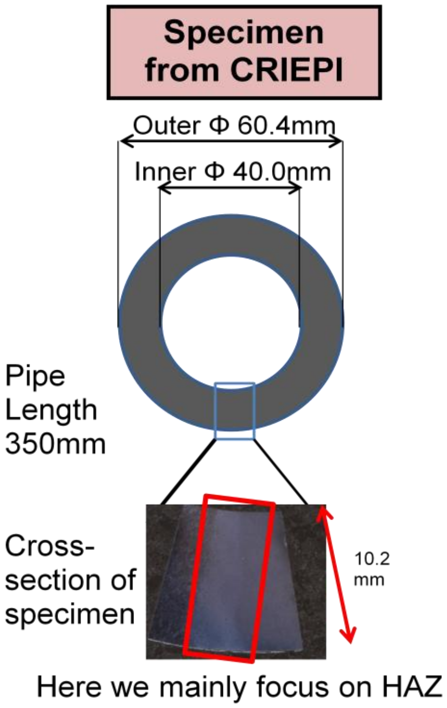

↑ Fig.3.1d measurements on specimen

3.2 Internal pressure creep experiment

The internal pressure creep experiment on Mod. 9Cr-1Mo steel was performed in the machine shown in fig. 3.1b. The specimen was heated by electricity and applied pressure by steam. Temperature distribution in radial axis is that distance $\pm 100\text{mm}$ further away from the center of the tube had temperature only 1°C different from the center. The temperature in the experiment was adjusted to match the temperature in the actual environment at 650°C, pressure is controlled between 25.6 MPa to 17.5 MPa(Mean value of radial stress 64.0 MPA to 43.8 MPa). The rupture time of the specimen was marked at the time leak of steam was spotted. Referring to the rupture time, 56% creep damage specimen was created by applying internal pressure of 21.7 MPa (average radial pressure of 54.3 MPa) to specimens for 6700 hours.

3.2.1 Characteristic of internal pressure creep hardness

The result of longitudinal welding creep of internal pressure uniaxial creep test specimen is shown in fig. 3.1c. The stress applies in internal pressure creep test is represented byσ_n, and is so far calculated by the usage of uniformed uniaxial stress.

$$\sigma_n = p(\frac{D}{2t} - y) \tag{3.2.1.1}$$

, where p is internal pressure, D is the external diameter of the tube. t is the thickness of material, y is a constant, with average value of 0.5. From the result of uniaxial internal creep test the compatible value of y is 0.38. [2] From the graph in fig. 3.1c, the bold line was the plot of the result from mod.9Cr steel weld-joint uniaxial creep test in base metal area. The thin line is taken from the weld-joint area. The weld-joint specimen under internal pressure of 21.7MPa and has rupture time of 6700 hours is shown in fig.3.1c.

3.3 Material Preparation

The specimen received from Central Research Institute of Electric Power Industry was a cross-section of gas tube containing base metal, heat affected zone, and weld metal as fig. 3.3.1 shown below. The specimen was then mounted into resin for convenience of inspection and planarizing. Resin mounting press instrument used in this process is Struers CitoPress-1 as showed below in fig.3.3a. The resin type in heat press was PolyFast from the same maker, Struers. The diameter of the resin cylinder is 25mm. Next, to prepare specimen for scanning electron microscope, first we needed to planarize the surface of the specimen by diamond polishing and oxide polishing which would be explained subsequently.

↑ Fig.3.3 Automatic resin mounting press, Struers CitoPress-1

3.3.1 Surface Polishing

Surface polishing process was conducted at National Institute of Occupational Safety and Health, Japan. The polishing machine used in this process is Struers Tegrapol-21. Polishing procedure started from polishing for 1 micro meter with diamond polishing for 10 minutes to level the surface. Then, conduct polishing again with OP (oxide polishing) for another 10 minutes. For oxide polishing, certain materials, especially those which are soft and ductile, require a final polish for optimum quality. Here, oxide polishing is used. Colloidal silica, with a grain size of approximately 0.04 μm and a pH of about 9.8, has shown remarkable results. The combination of chemical activity and certain abrasion results in scratch-free, deformation-free specimens to be observed in microscopic level. OP-A, is used for final polishing of low and high alloy steels, nickel-base alloys and ceramics.

↑ Fig.3.3.1 Surface polishing instrument, Struers Tegrapol-21

↓ Table 3.3.1 methods and solutions employed in polishing process

DP: Diamond Polishing (1 μm)	MD Dac (abrasive grain: diamond, 9-1 μm) Abrasive solution : DP-Suspension, 3 μm Lubricant : DP-Lubricant, Green
OP: Oxide Polishing	MD Chem Abrasive solution : Colloidal Silica (OP-U,0.04 μm)

3.3.2 Surface Corrosion: Etching

Surface polishing accomplished a goal to planarize surface of the material in a preparation to capture the heat-affected zone's surface with scanning electron microscope. Yet, the disadvantage of surface polishing is that the visible trace of heat affected zone on the surface of the specimen and the grain boundary traces are also eradicated, leaving only monotonously silvery surface. As a result, the research on several parameters of heat affected zone of the Mod. 9Cr steel cannot be accurately and specifically accomplished. Here, a method, called 'etching', was conducted to highlight grain boundary of material. Especially finer grain boundaries located in heat affected zone become visible after chemical corrosion process.

The chemical used in this process was a highly corrosive mixture of acid, Aqua Regia or, Ou-sui in Japanese. The mixture was formed by freshly mixing concentrated nitric acid and hydrochloric acid in a volume ratio of 1:3, respectively. The saturated solution was then dissolved in water 5% (w/v). The surface of newly polished specimen was immersed in the thinned aqua regia solution immediately for 50 seconds to induce corrosion, then, thoroughly rinsed in water. Heat affected zone normally becomes prominently visible after this corrosion process. Other known corrosive substances of mod.9Cr-1Mo steel are Nital solution (combination of nitric acid and alcohol) and picric acid.

3.4 SEM image processing

After specimen had been polished, oxidized polished, and corroded, it was directly taken to a vacuum chamber to have its surface measured by scanning electron microscope. The vacuum chamber protected it from natural oxidization on the steel's surface and ensured the quality of the scanning electron microscopic photographs. The specification of the SEM machine and the observation conditions were listed below in table3.4.

↓ Table 3.4 SEM machine and the observation conditions

Scanning Electron Microscope	KEYENCE VE9800
Magnification	500 times
Working Distance(mm)	8
Spot Size(mm2)	8
Accelerating Voltage(kV)	10.0
Observation size(μm^2)	240x180

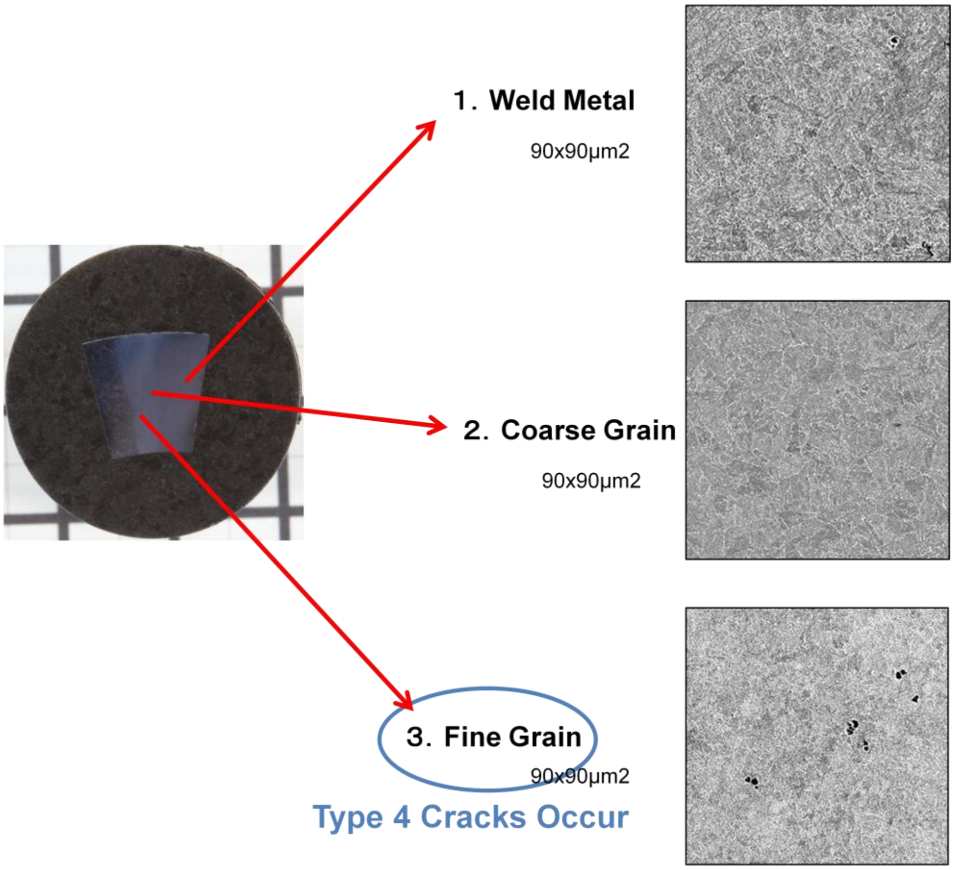

↑ Fig.3.4a sample of SEM images on various areas

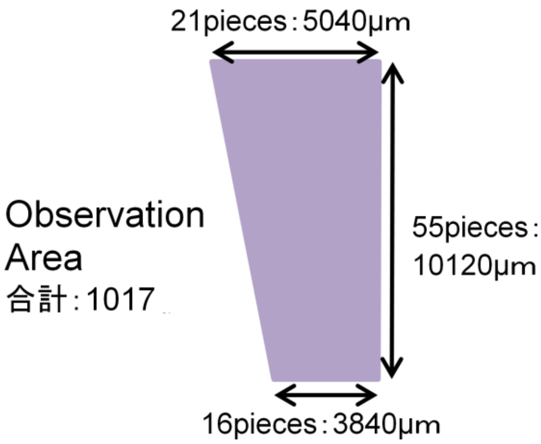

↑ Fig.3.4b measurement of observation area.

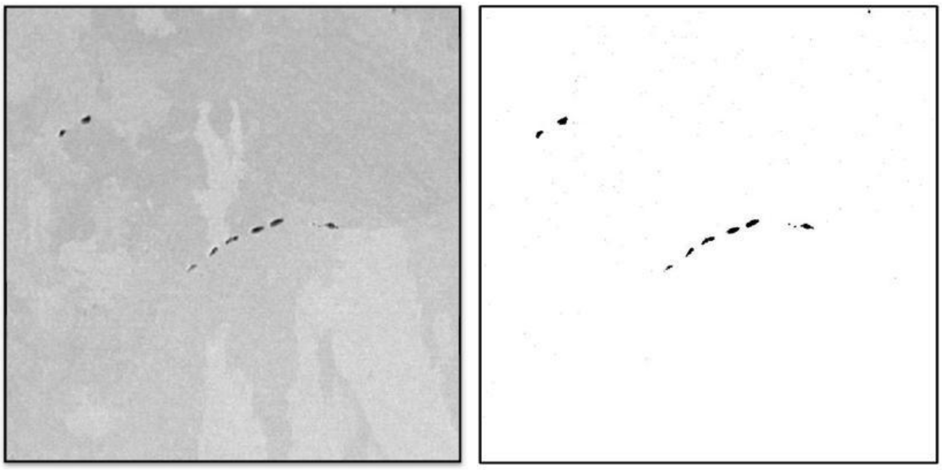

↑ Fig.3.4c binarisation and noise reduction of SEM image

Scanning electron microscope is used in this research for two principal reasons: to study the spatial distribution of creep void in the heat affected zone and to observe the grain size of base metal, weld metal, coarse grain size area, and fine grain size area.

Since the target of this observation is generally in the heat affected area, first we covered the rest of the surface of the specimen with carbon tape, leaving only white line in the middle identified as heat affected zone.

The movement of the motor of SEM microscope was not considered that precise; therefore, there was possibility that the pictures captured by scanning electron microscope might be overlapped in the ridge area. We perform a method to ascertain that we remove the double creep voids on the edges. To make it easy to recognize the overlaps, we merge the edge of each picture together by using an image processing program to knit them together vertically. Each vertical line of SEM photographs consists of 50 pieces. Then, we go through them in order, and check whether there are double points to delete. The description of this method is explained below in fig.3.4b. After checking for doubles voids, we separate each photographs and finally before binarising each photograph, creep void verification was conducted.

Creep void verification was mandatory since the black dots on the surface of the specimen might not all be creep voids. The criteria used in this verification were hold confidential by Central Research Institute of Electric Power; therefore, we would like to skip this area to the result.

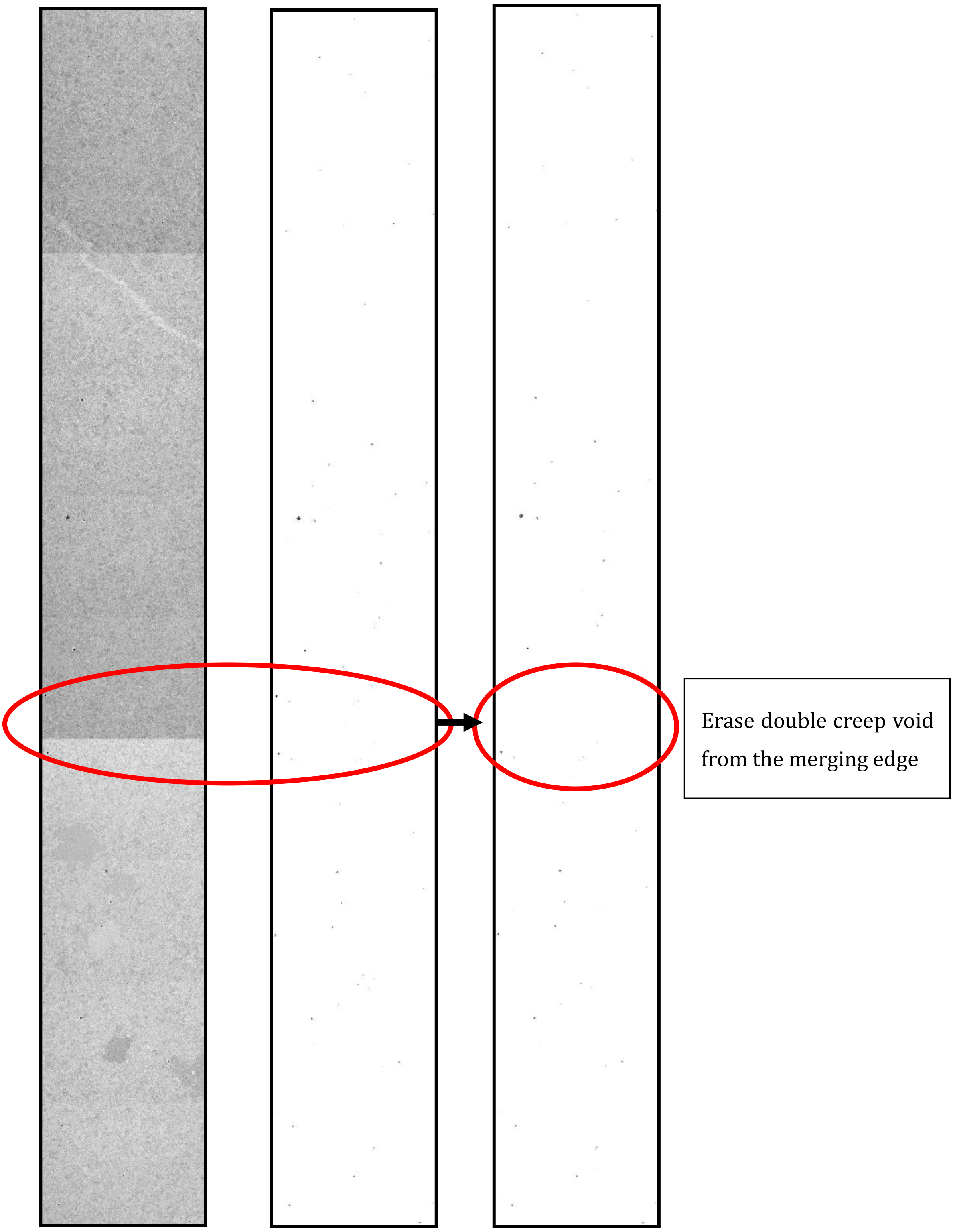

↑ Fig.3.4d basic method of merge and check process

3.5 Void Area Ratio and Image processing

When creep void check was done, we binarised each photograph one by one into black and white image by image processing software, IMAGEJ. Threshold was then adjusted to filter unfavorable noise. The less noise means it is easier for the software to do the void counting. Function analysis of IMAGEJ not only allowed us to count the number of clusters of dark pixels but also helped calculate the amount of black pixels itself, which means void area ratio can be easily acquired. Thus, IMAGEJ actually saved us a great amount of time in analysis.

The definition of creep void area ratio is as equation (3.2.1.1) below.

$$\text{void area ratio} = \frac{\text{void area(black pixels)}}{\text{total area(whole photograph pixels)}} \tag{3.2.1.1}$$

Creep void area ratio and void distribution are both ranked top four of the criteria used to identify creep damage area. Those four criteria include:

1.) Void area ratio

2.) Void grain boundary dominant ratio

3.) Void distribution

4.) Void size

Here we exercised void distribution and void area ratio because those two criteria are considerably straightforward for statistic analysis in form of spatial distribution in specific area which is heat affected zone.

3.6 Grain Size Measurement

Type IV crack is believed to found primarily in a specific area of heat affected zone called, fine grain area. Thus, it is important that we are capable of distinguishing types of surface of the area, which fundamentally comprise of four types: weld metal, base metal, coarse grain, and fine grain, as larger to smaller grain size respectively. The information concerning grain type is therefore mandatory if an analysis on creep generating process should ultimately be accomplished. SEM images are viewed one after another in vertical order to define the grain type characteristic of each image.

Numerical criteria used to distinguish grain type are listed below in table 3.6a.

↓ Table3.6a numerical criteria to distinguish grain type

Grain type	Approximate grain diameter(μm)
Weld metal	100-250
Base Metal	50-120
Coarse grain	30-80
Fine grain	5-20

From observation, there might be numeral types of grain in one image. For instance, around the boundary of fine grain area and coarse grain area is shown in contour graph in fig.5.1.1a in Chapter 5 or in SEM photograph in fig. 3.6 below. Considering fig. 3.6, we judged that whole area of fig. 3.6 to be coarse grain because the coarse grain covers most of the total area. With this simple rule, the whole observation surface is transformed into a single distribution called grain type distribution (fig. 5.1.1a).

Here, by highlighting the grain type boundary out of the whole distribution we hope to procure a mask that after patching on other distributions of the same observation area, such as creep distribution, creep void area distribution, Vickers hardness distribution, we can define certain property of each grain type, and perhaps are able to focus specifically on fine grain area where most of the type IV cracks are located.

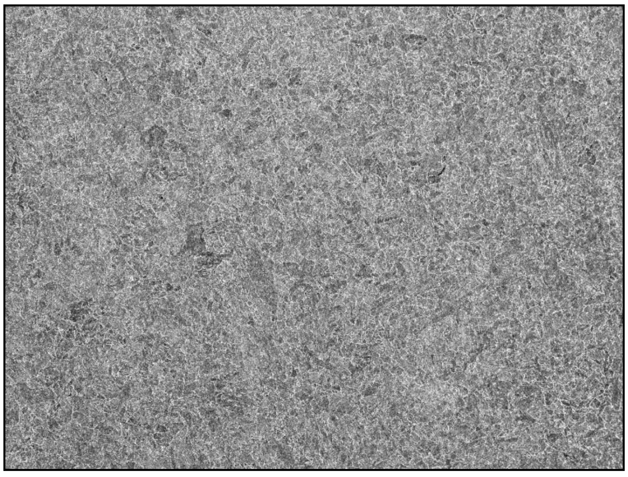

↑ Fig. 3.6 an area containing both fine grain and coarse grain

3.7 Vicker's Hardness

The history of Vickers Hardness goes back to year 1921 when Robert L. Smith and George E. Sandland, working as material engineers at Vickers Limited, had invented an alternative way to the Brinell method to measure the hardness of materials. The Vickers test is regularly less complex and simpler to practical use than other hardness tests such as Brinell, Meyer, Rockwell since the required calculations are not dependent on the properties of the indenter. Furthermore the indenter can be applied to all materials despite their hardness. There are, however, some fundamental principles concerning common measures of hardness that should be clarified. One is to observe the test material's ability to resist plastic deformation from a standard source. The Vickers hardness test can theoretically be used for every kind of metals and undoubtedly has one of the largest scales among the hardness tests. The unit of hardness given by the test is known as the Vickers Pyramid Number(HV) or Diamond Pyramid Hardness (DPH), which can be converted into units of Pascals. Nonetheless, this Pascal unit should never be confused with pressure, which also has units of Pascals. The hardness number is determined by the load over the surface area of the indentation and not the area normal to the force, and therefore should not be considered a pressure.

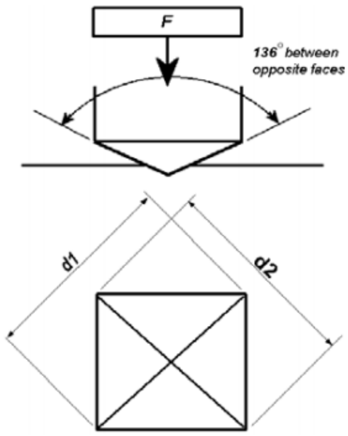

↑ Fig.3.7a Vickers hardness test scheme[10]

The hardness number is not really a true property of the material and is an empirical value that should be seen in conjunction with the experimental methods and hardness scale used.

In normal Vickers hardness test, we utilize a press of which head (indenter) is made of diamond in the form of a square-based pyramid like the one showed in fig.3.7a above. It had been acknowledged that the ideal size of a Brinell impression was 3/8 of the ball diameter. And because two tangents to the circle at the ends of a chord 3/8 of diameter long intersect each other at 136°, it was then determined to define that number as the included angle of the indenter. Then, there were experiments on different angles and, to their surprise, it was established that the hardness value obtained on a homogeneous piece of material remained constant, irrespective of load.

Hence, loads of various magnitudes are applied to a flat surface, depending on the hardness of the material to be measured. The HV number is then determined by the ratio *F/A* where *F* is the force applied to the diamond in kilograms-force and *A* is the surface area of the resulting indentation in square millimeters. Area, *A*, can be determined by the following formula

$$A = \frac{d^2}{2\sin\left(\frac{136^\circ}{2}\right)} \qquad (3.7.1)$$

, where *d* is the average length of the diagonal left by the indenter in millimeters.

$$HV = \frac{F}{A} \approx \frac{1.8544F}{d^2} \qquad (3.7.2)$$

, where *F* is in kgf and *d* is in millimeters.

The condition of Vickers' Hardness measurement in this experiment is listed in the table below in table 3.7a.

↓ Table 3.7a micro Vickers hardness instrument specification and condition

Hardness Measurement Instrument	FISCHERSCOPE HM2000
Load	10.0 N
Initial Load time	10s
Secondary Load time	10s

In addition, the image of the measure instrument in shown in fig. 3.7b. Since the advantages of Vickers hardness machine are the extremely accurate readings of results comparing to the Brinell or Rockwell hardness especially when it comes to measuring the softest and hardest domains of specimen; the Vickers hardness machine is normally a floor standing unit which is known to be more expensive than other hardness test machines.

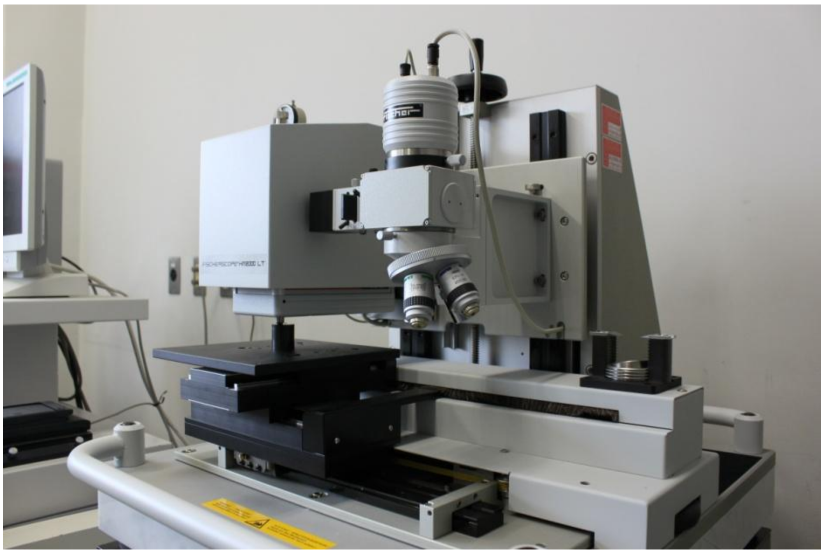

↑ Fig. 3.7b hardness measure instrument

The results of Vickers hardness were taken twice: first time covering the surface area of the whole specimen and the second time focusing only on the observation area especially where fine grains were located. There are many benefits of conducting the test twice at different scale. Firstly, it is to ensure that the Vickers hardness result is actually accurate and reliable. Secondly, it is important to observe a larger surface to comprehend the whole grain boundaries while a narrower version only focuses on the specific area of SEM observation. The grain type boundary mask we procured from grain type distribution can be of best use in the narrower perspective only.

Chapter 4: Finite Element Method Analysis

Here we created two-dimension simulation model of creep-rapture both based on finite element analysis. The model was created using plane strain element (PLANE183) on ANSYS11.0. The reason why plane strain was chosen instead of plane stress was that the model actually had significantly small base size comparing to its length. In this case the outer radius of the tube was 30mm while the length of the tube was 350mm. In addition, since internal pressure only worked in x-y plane, we considered strain in z axis equal to zero.

Three-dimension analysis can also be simulated, but since answers were supposed to be the same we chose the simpler method of the two. Internal pressure creep simulation condition and meshing condition is showed below in fig.4.1a, fig.4.1b and table 4.1a.

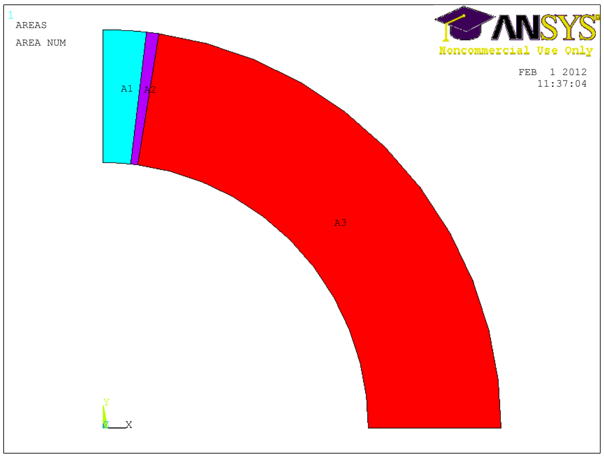

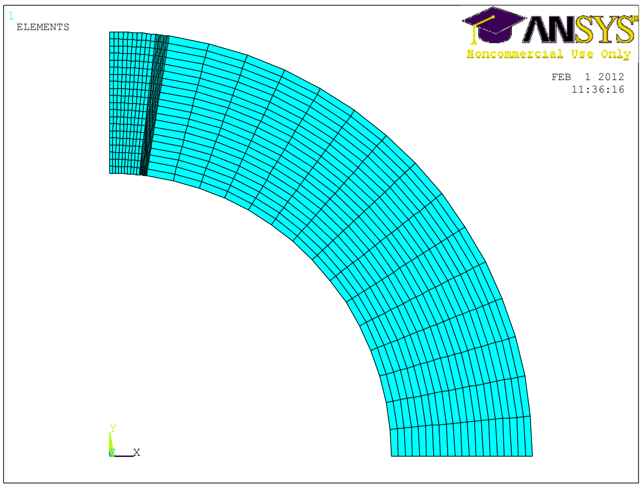

↑ (Left)Fig.4.1a modeling of heat affected zone of mod.9Cr steel boiler pipe

↑ (Right)Fig.4.1b meshing of heat affected zone of mod.9Cr steel boiler pipe

↓ Table 4.1a two-dimension modeling details

Two-dimension Modeling Detail	
Model Symmetry	1/4 of full object
Pipe Outer Radius	30mm
Thickness	10mm
Internal Pressure	Inner 21.7MPa

Temperature	constant at 600℃
Creep time	6700 hours
Element number	700
Node number	2211

We previously introduced the creep strain rate calculation once in chapter 2. Creep strain rate equation by Norton Law is listed below in equation 2.1-3. And the table 4.1b shows the values of variables used in this analysis. The source of these figures was from simulation experiments on mod.9Cr steel by Central Research Institute of Electric Power Industry. In addition, since the creep strain property of coarse grain area in HAZ was significantly close to the property of weld metal. We treated coarse metal area as a part of weld metal. Thus, in table 4.1b, only fine grain area was the representative of heat affected zone.

$$\dot{\varepsilon}_c = B\sigma^n \qquad (2.1\text{-}3)$$

Material	E (Mpa)	N	B	N
Base Metal	164000	0.3	5.39×10^{-18}	6.53
Weld Metal	117000	0.3	3.75×10^{-18}	6.53
Fine(HAZ)	124000	0.3	2.66×10^{-16}	6.53

↑ Table 4.1b material properties

Chapter 5: Results and Discussion

This chapter consists of the results of all measurements in this research. Firstly, we would like to introduce the result of the observation of heat affected area of mod.9Cr steel by scanning electron microscope, which included contour graphs of creep void distributions, creep void area ratio, grain type, and each of the previous graphs with grain type boundary mask lying on top. The benefit of contour graph is that it is easy to comprehend, easy to recognise patterns, and suitable for distinguish differences in specific locations. We also converted the data in contour graphs of creep void distributions and creep void area ratio into line charts for vertical and horizontal axis analysis. Note that line charts are not capable of demonstrating data on both axises at the same time. However, the direction of creep void density we found in contour graph can be confirmed by referring to line charts.

Additionally, contour graph is the key to our destination to divide the observation area by grain types and plot lines on those boundaries. These boundary lines would ultimately prove whether creep void were actually dense in fine grain area, whether creep void area ratio were high in fine grain area, whether the surface was hardest in weld metal and spongiest in fine grain area. These are very interesting questions that have yet been statistically confirmed yet. These results would elucidate the doubts in creep void mechanics in mod.9Cr steel. Nonetheless, without theoretical explanation, confirmation by observation alone can be regarded disputable.

Here, we supplementarily performed finite element method (FEM) analysis simulating the experiment condition of the specimen. Focusing on triaxiality factor to be the pivotal cause of creep damage, we measured all three principal stresses and von Mises stress, calculated the triaxiality factor and replotted it on the surface. The result showed unquestionably strong relation between triaxiality factor and creep void spatial distribution, while creep strain rate did not show significant relation with the amount of creep voids.

5.1 SEM observation result

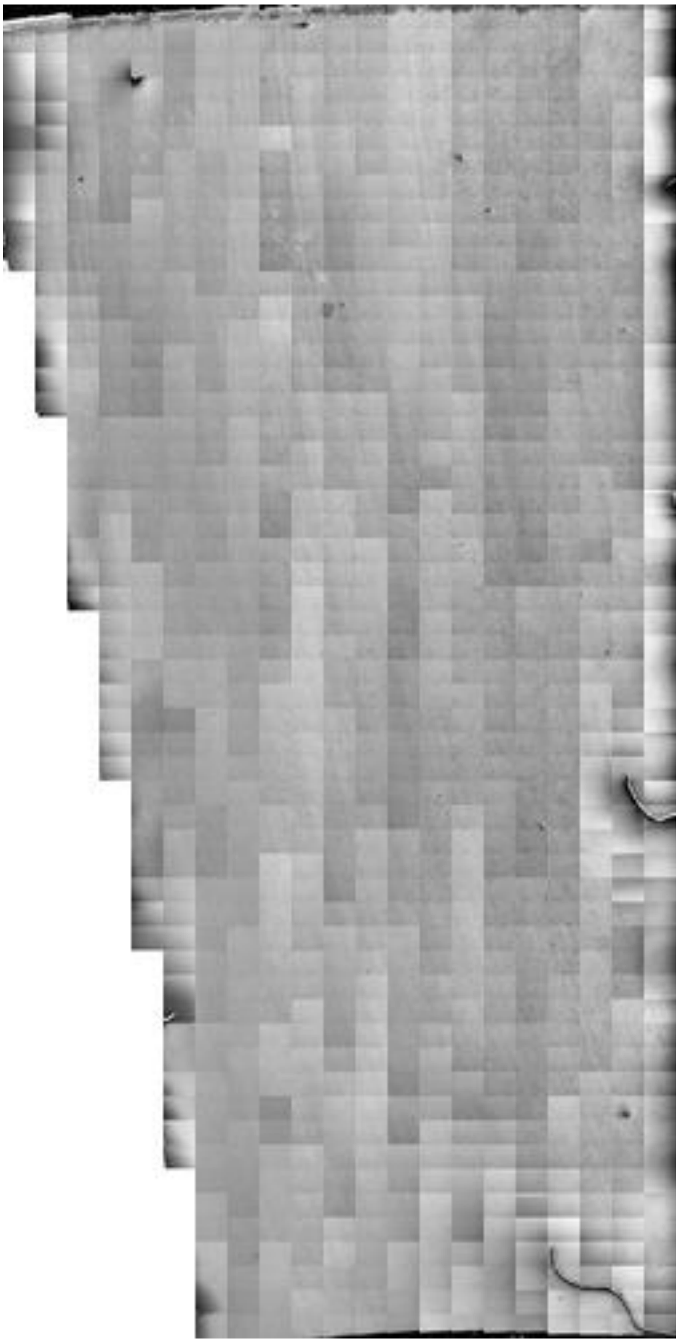

↑ Fig. 5.1a the total SEM photographs stitched together

5.1.1 Grain Type Distribution

As mentioned in chapter 3, grain type distribution is considered the most pivotal element in this research due to the clarity of the information we have that creep damage is mainly found in fine grain area of the material. The reason, for now, is unclear why the creep-rupture strength in the area has been degraded, but that is supposed to be clarified by the result of finite element method to be mentioned later in this chapter.

The criteria we used to separate each grain type are also mentioned in Grain Size Measurement Method in Chapter 3.6. Grain size is the how we divide fine grain from coarse grain, weld metal, and base metal. The result of grain type distribution based on grain size is as showed in fig. 5.1.1a below.

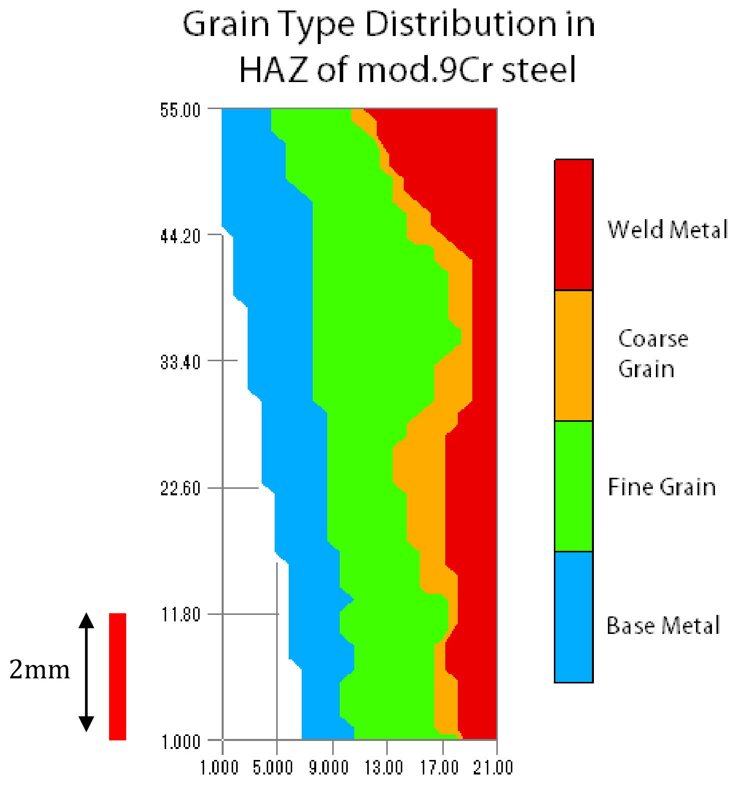

↑ Fig. 5.1.1a grain type distribution in HAZ of 56% damaged specimen

From fig.5.1.1a, it is obvious that the boundary of weld metal, coarse grain, and fine grain area are not a straight line comparing to the boundary between fine grain and base metal. By definition, heat affected zone is an area of base metal where heat, transferred from weld metal, has altered its microstructure and properties. The size, the new properties are basically based on thermal diffusivity of the base material, the weld material, and the amount of heat in the welding process. The thermal diffusivity of the base metal is believed to play an important role. If thermal diffusivity is high, the material tends to cool down fast, which resulting in relatively small heat affected zone. On the other hand, base material with low diffusivity has slower cooling rate and larger heat affected zone.

The reason why there are two different types of heat affected zone is because the time span available for cooling is different depending on how close to the high temperature weld metal. Heat affected zone closer to base metal can transfer heat easily while the area closer to weld metal has been heated repeatedly. When crystallization process occurs, the areas with higher cooling rate don't have much time to composite large crystals, ultimately resulting in fine grain area. Relatively narrow areas next to weld metal have a different story. Those areas have considerably long period to re-crystallize, ending up with comparably large grain size, called coarse grain area.

By creating outlines in the grain type contour graph, we procure a tool, grain type boundary mask, to distinguish grain type in any contour distributions based on the observation area of the same coordinate system which in this research refers to creep void density distribution, void area ratio distribution, and Vickers hardness distribution. For Vickers hardness, we conducted the measurement on a different instrument; as a result, although we try to focus on the same area of the surface with the help of visible white stripe on the surface thanks to corrosion process, the coordinate systems are totally different, and there can possibly cause some minor offsets.

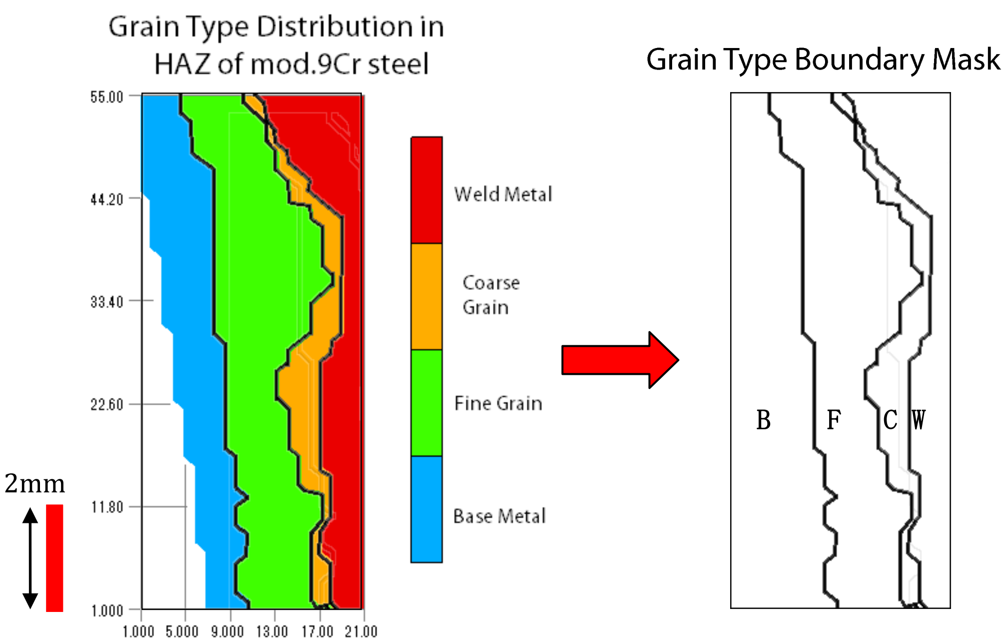

↑ Fig.5.1.1b transition from grain type distribution to grain type boundary

5.1.2 Creep Void Density Distribution and Area Ratio Distribution

The data of creep void density distribution was taken from all scanning electron microscope of total of 1017 photos. Each photograph represented one node of the distribution. Starts from marine blue to red, the amount of creep void density became respectively larger. The result is showed below in fig. 5.1.2a. It is relatively obvious that the highest creep density is located in the upper-middle in the vertical axis. And in aspect of the grain type, in fig. 5.1.2b, creep void can scarcely be found in coarse grain, weld metal, and base metal.

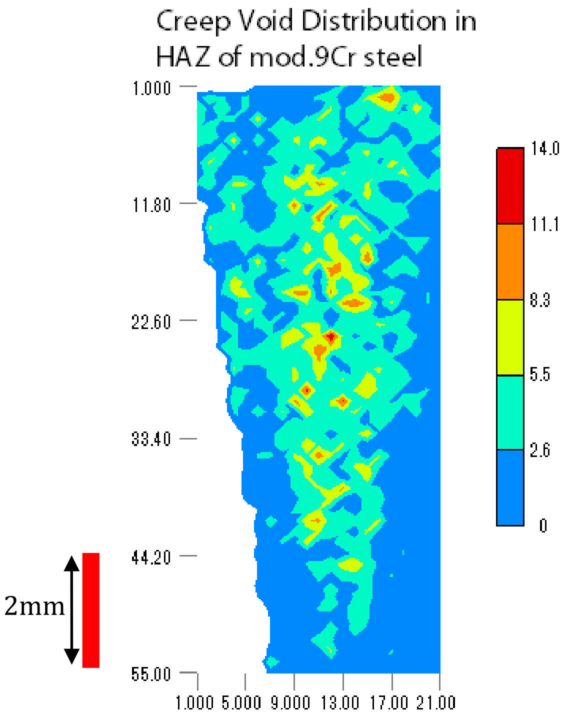

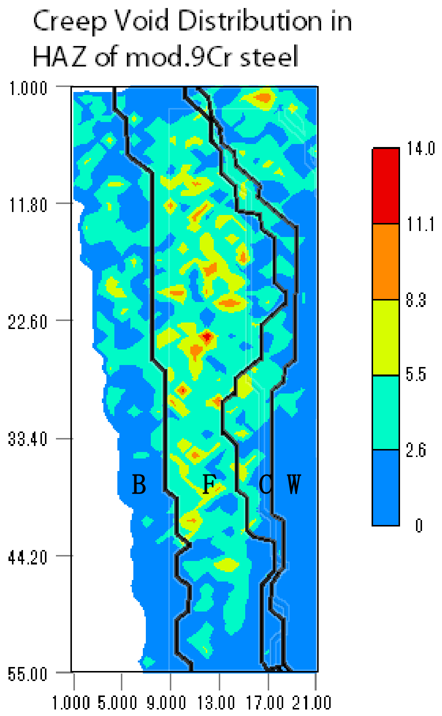

↑ (Left)Fig. 5.1.2a distribution contour graph of creep void density on the observation surface

↑ (Right)Fig.5.1.2b grain type boundary on creep void density distribution contour graph

Creep voids primarily locate in the center of the thickness axis and in fine grain area of the horizontal axis. Most of the surfaces of base metal and weld metal scarcely have any creep voids with an exception of the region close to outer surface. Comparing to weld metal surface, base metal surface obviously has higher average creep void density, which spread throughout its thickness. Meanwhile, coarse grain area does not have significantly large number of creep voids. By contrast, coarse grain area tends to have even less creep voids than base metal.

To scrutinize the distribution of creep void density in questionable fine grain area quantitatively, we selected the data from the photos with fine grain area type (with reference of data in fig. 5.1.1a), and calculated the average value of amount of creep voids and the standard deviation horizontally and vertically. Vertical quantitative analysis is showed below in fig.5.1.2c and in Graph 5.1.2a

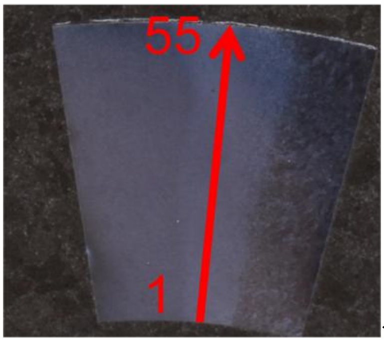

←Fig.5.1.2c creep void amount vertical quantitative analysis

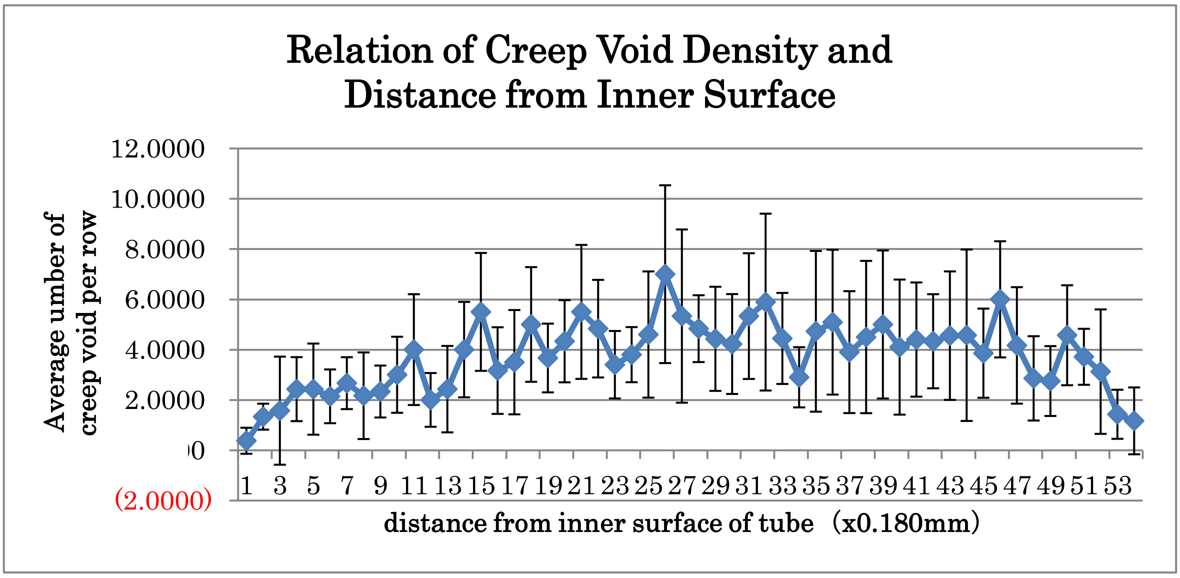

↑ Fig. 5.1.2d result of creep void amount vertical quantitative analysis

Fig.5.1.2c we conducted a statistical calculation on the amount of creep voids per each row of SEM photographs. Each row of SEM photographs, only the photographs considered as fine grain area were included in the calculation. Another version of calculation was conducted but the graph result included too wide standard deviation. According to fig. 5.1.2d above, Creep voids are densely located in the central and outer surface of the steam pipe. The highest mean value is at row 27th which is in the very center of the observation axis.

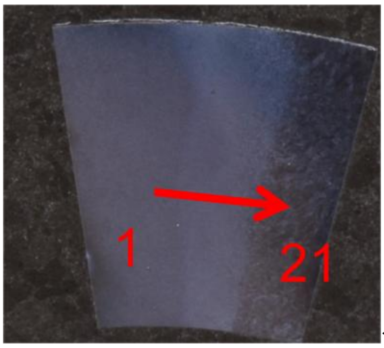

←Fig.5.1.2e creep void amount horizontal quantitative analysis

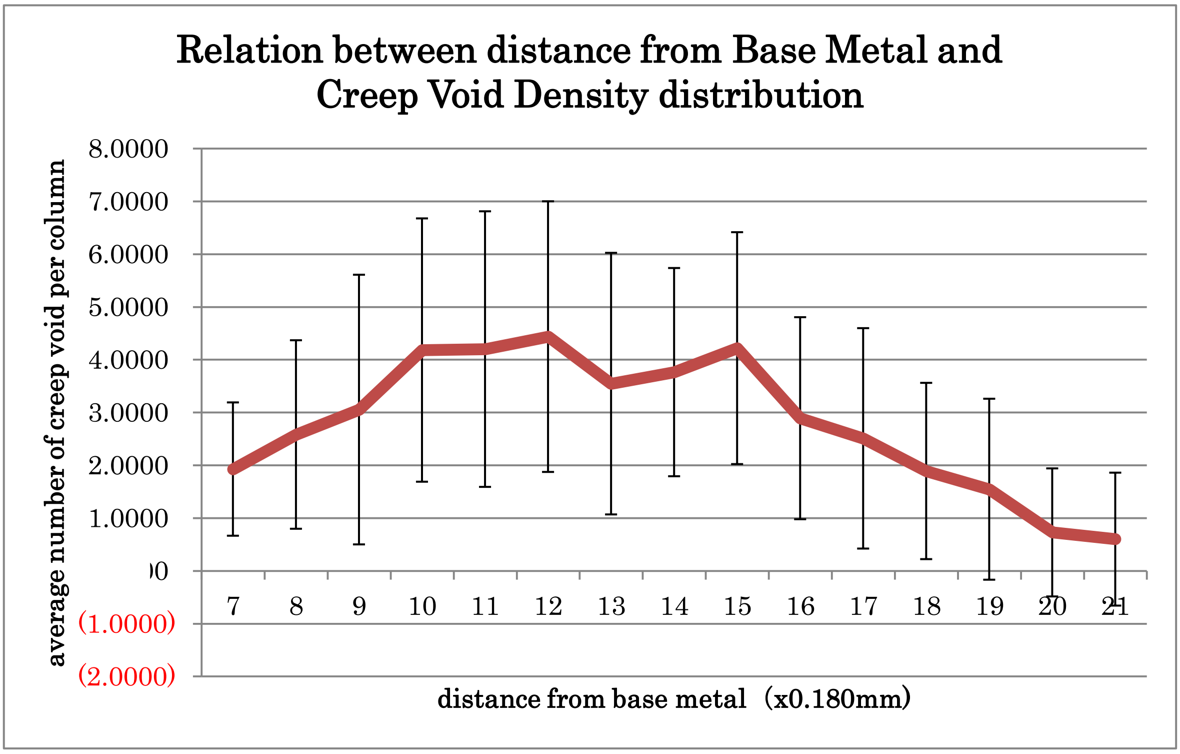

↑ Fig. 5.1.2f result of creep void amount horizontal quantitative analysis

On the other hand, fig.5.1.2e we conducted a statistical calculation on the average amount of creep void per each column of SEM photographs. As the observation area was in a shape of trapezoid, some of the areas especially to the left end were not qualified for statistical calculation. According to fig. 5.1.2f above, Average amount of creep voids is highest in row12th, following by 15th and 10th, while fewer voids were found the closer to weld metal we proceeded. Column 21st had average of approximately 0.6 Note that from mod.9Cr steel grain size distribution, fine grain area situated in column 10th-17th. The highest mean value is at row 27th which is in the very center of the observation axis.

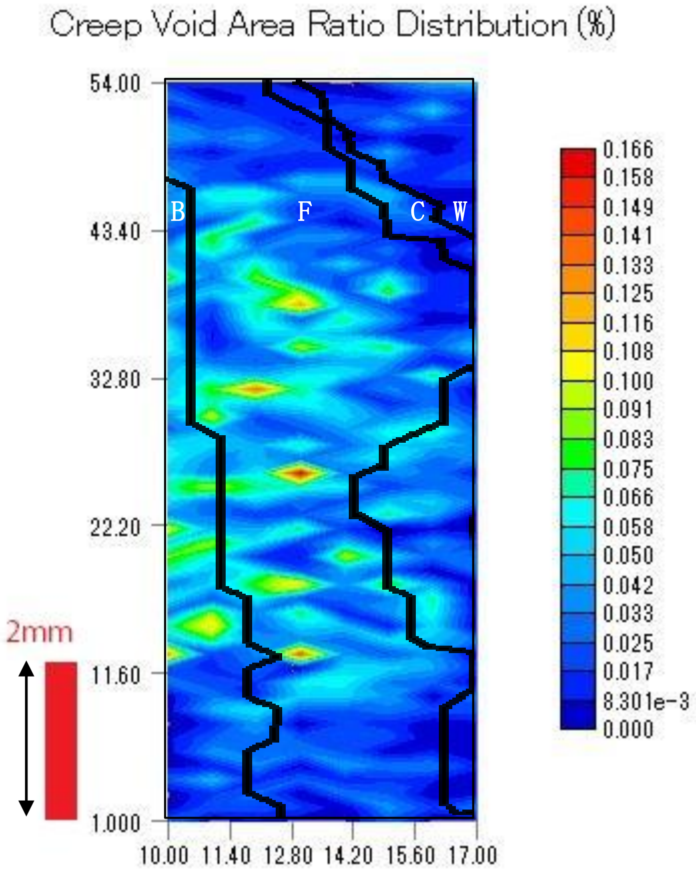

↑ Fig. 5.1.2g distribution of creep void area ratio with grain type boundary

Void area ratio is another criterion to determine creep damage on a surface of steel. The method of this process and how the calculation was conducted have been mentioned back in Chapter3.5. Anyhow, fig. 5.1.2g shows that high creep void area ratio establishes at the center of observation area and somewhat to the base metal side on the left. From scanning electron microscopic photographs, it is obvious that creep damage is extremely scarce in weld metal area. Therefore, the right side of this contour graph is rather unoccupied.

There are approximately 5 peaks where creep void pixel numbers rise over 1300 pixels and are showed in orange and red color. Four out of five peaks are located in fine grain area, while the other one is in base metal area. Void area ratio, unlike creep void distribution contour figure, hardly has any high results on both upper and lower ends of the distribution.

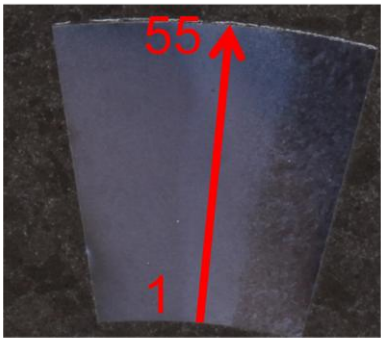

←Fig.5.1.2h creep void area ratio vertical quantitative analysis

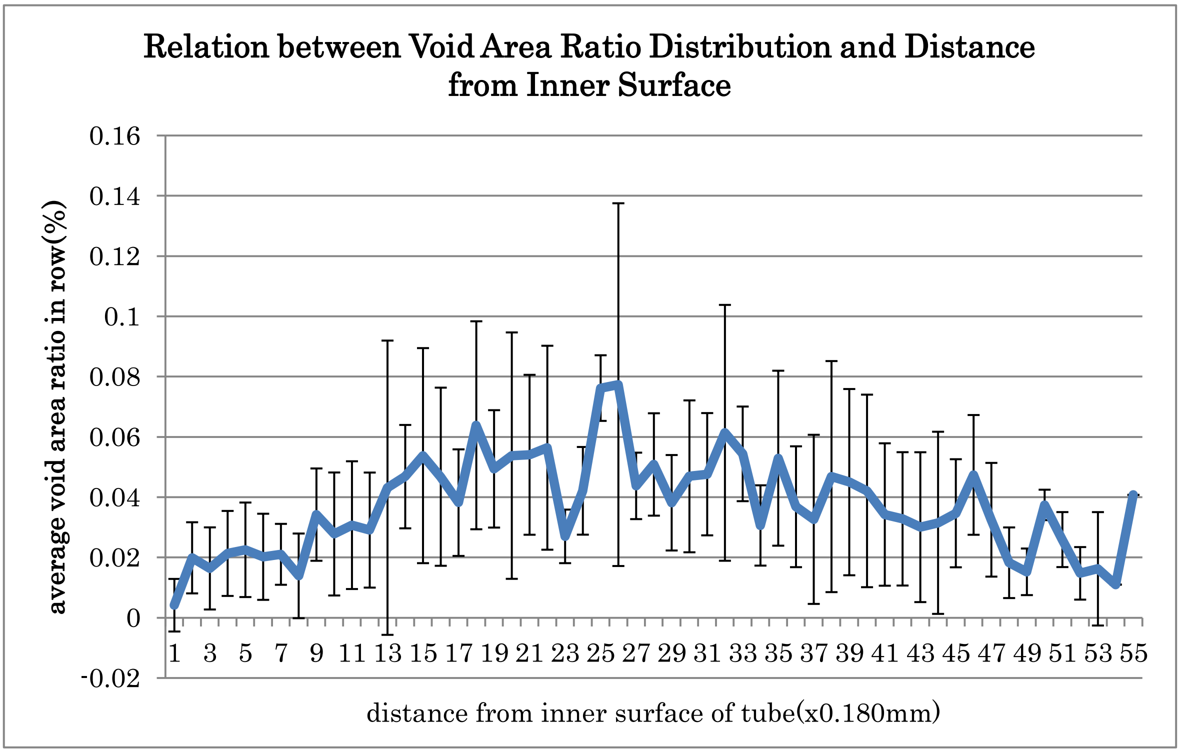

↑ Fig. 5.1.2i result of creep void amount horizontal quantitative analysis

Fig.5.1.2h we conducted a statistical calculation on the creep void area ratio per each row of SEM photographs. Each row of SEM photographs, only the photographs considered as fine grain area were included in the calculation. According to graph5.1.2i above, Average creep void area ratio is highest in the central surface of the steam pipe in vertical axis. The highest mean value is at row 26th, 18th, 32th respectively. The sample space of this data set is wide throughout the graph except for the very right end of this graph. In other words, there was a lack of number of data on row 54th-55th, causing the result to become fluctuating.

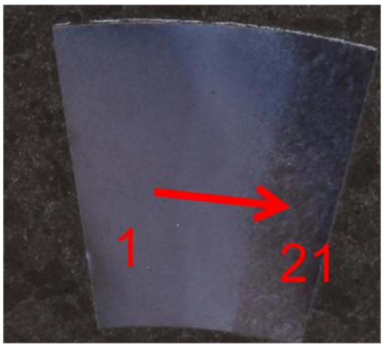

←Fig.5.1.2j creep void area ratio horizontal quantitative analysis

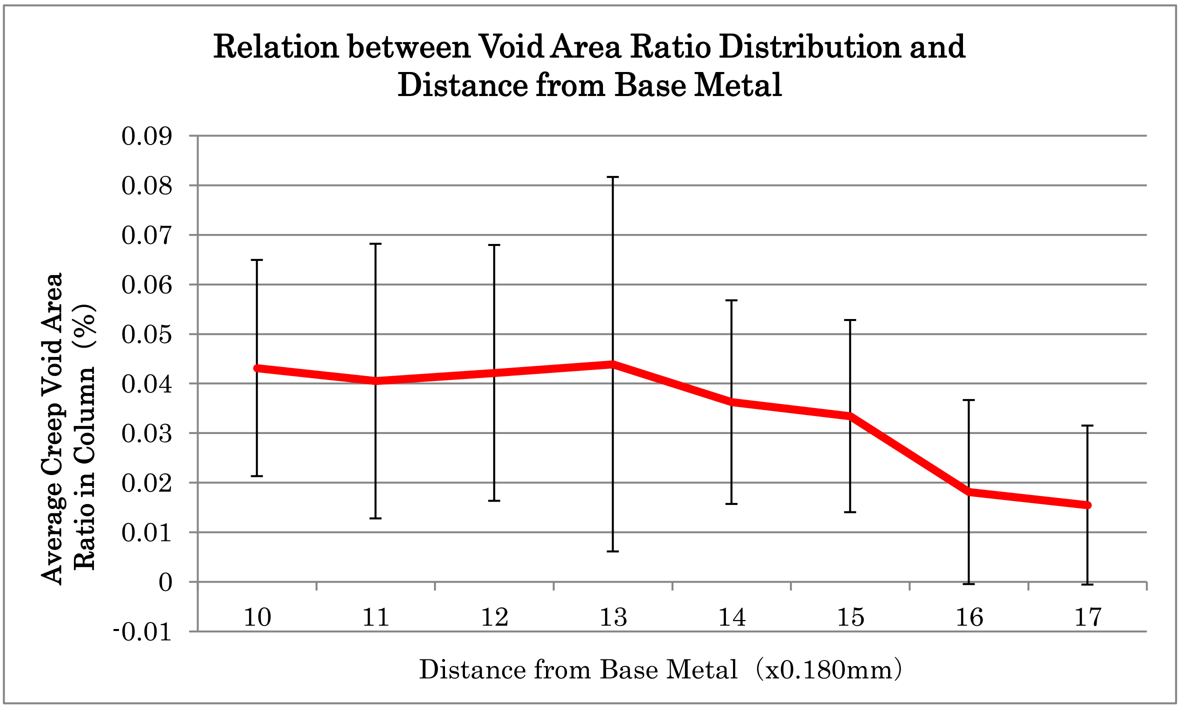

↑ Fig. 5.1.2k result of creep void amount horizontal quantitative analysis

On the other axis, fig.5.1.2j we conducted a statistical calculation on the average amount of creep void per each column of SEM photographs. Similar to the result on vertical axis of creep void distribution in fig. 5.1.2k, as the observation area was in a shape of trapezoid, some of the areas especially to the left end (column 1-9) were not qualified for statistical calculation, while the columns on the right (column 18-21). Regarding fig. 5.1.2k above, average amount of creep voids is highest in row 13th, following by 10th and 12th, while fewer voids were found as we approached weld metal. Column 17th had the least average of approximately 0.016%. Note that from mod.9Cr steel grain size distribution, fine grain area situated in column 10th-17th, and especially the columns on the right were generally mixed with coarse grain area and weld metal, resulting in fewer creep voids and smaller sample space.

5.1.3 HAZ Vickers Hardness

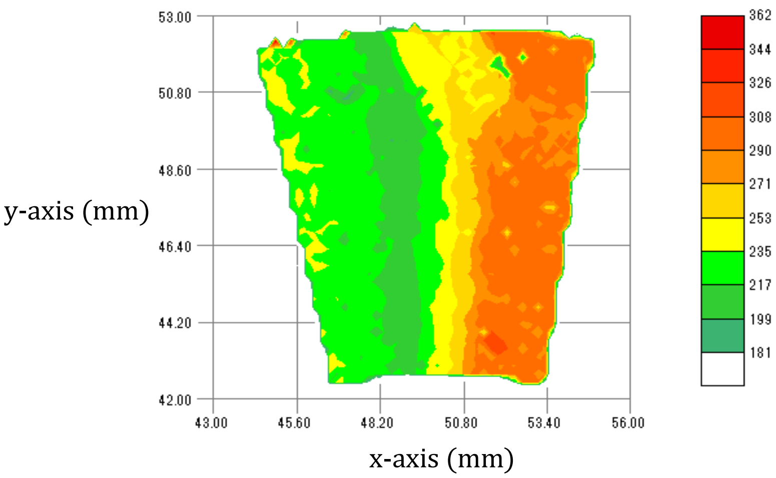

↑ Fig.5.1.3a result of Vickers hardness of surface of specimen

Vickers hardness of mod.9Cr steel was previously showed in a graph in fig.3.1a. A brief transition of hardness in the center of the contour graph is significant in this research. First question is where fine grain area and coarse grain area are located in this graph. Without a appropriate tool, the question will never be answered. We already knew from the optical image in fig. 3.4a that heat affected zone where fine grain area is located is in the very center of the specimen's surface. Considering fig. 5.1.3a above, there was a rather high possibility that fine grain area would be situated in the softest part of the contour graph. But, how could we be certain? How could we confirm the location of the fine grain in a totally different coordination system?

With grain type boundary mask we procured in chapter 5.1.1, the result became extremely prominent and straightforwardly comprehendible. The outcome of boundary grain type mask on Vickers hardness contour graph showed in fig. 5.1.3b below showed that the areas with the lowest Vickers hardness are mostly located in the fine grain area with some small proportion in base metal. The reason why the decline in hardness occurred in fine grain size and its consequences will be further discussed in chapter 6.

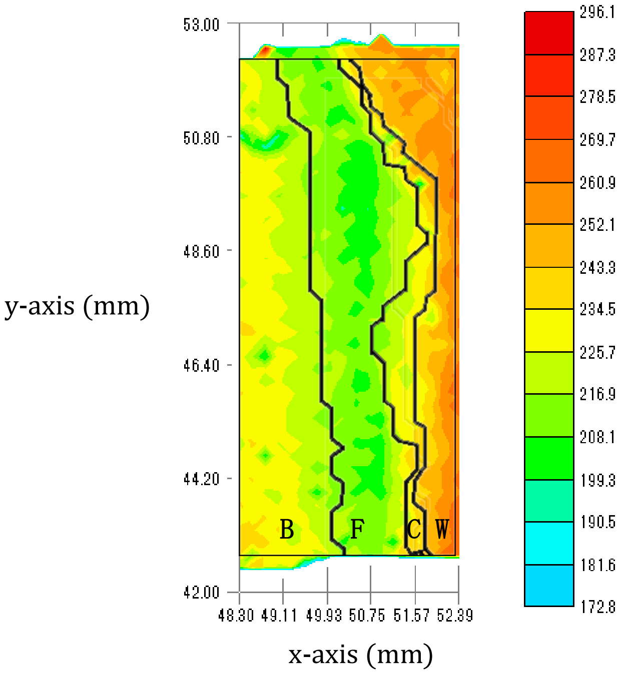

↑ Fig.5.1.3b result of Vickers hardness of HAZ with grain type boundary mask

5.2 FEM Analysis Result

Two-dimension analysis is proved significant in explaining the result of creep void in mod.9Cr steel specimen. Due to the very large proportion in z-coordinate direction of the specimen comparing to its small cross-section size, we used plain strain element to calculate the stress distribution and creep strain rate distribution. In addition, the applied pressure only worked in x-y plane and was constant in the z direction, so plain strain finite element analysis result should be the same as a three-dimension result.

Two-dimension results were listed below, including all three principal stresses, von Mises stress, triaxiality factor, and creep strain rate. All three principal stresses had particularly high value in heat affected zone, which made the sum even higher (fig. 5.2.1a, fig. 5.2.1b, fig. 5.2.1c). At the mean time, the center of heat affected zone had considerably low von Mises stress (fig. 5.2.1d). As a result, the value of triaxiality factor was most outstanding in the center of heat affected zone; furthermore, we also noticed that comparing area close to inner and outer surface of the heat affected zone, the inner surface had much lower triaxiality factor value than the outer part. These two characteristics were the very characteristics we derived from creep void distribution in fig. 5.1.2a and creep void area ratio in fig. 5.1.2e. This ascertained our hypothesis about the relation between creep strength plummet and high triaxiality factor.

In addition, the result of triaxiality factor distribution after 6700-hour simulation showed in 5.2.3e matches well with another creep void simulation conducted by Central Research Institute of Electric Power Industry in [8] with considerably high triaxiality factor value in heat affected zone 3/4 of the distance between inner surface and outer surface.

5.2.1 Immediately after the simulation started

Our first results were taken immediately after the simulation commenced at time = 10E-6. Fig. 5.2.1a and fig. 5.2.1b, it is obvious that in this situation, inner surface of the pipe has the highest value of principal stress and von Mises stress. Both value gradually increase as we get closer to the outer surface. Fig. 5.2.1c, since no significant amount of time has passed; creep strain cannot be calculated yet.

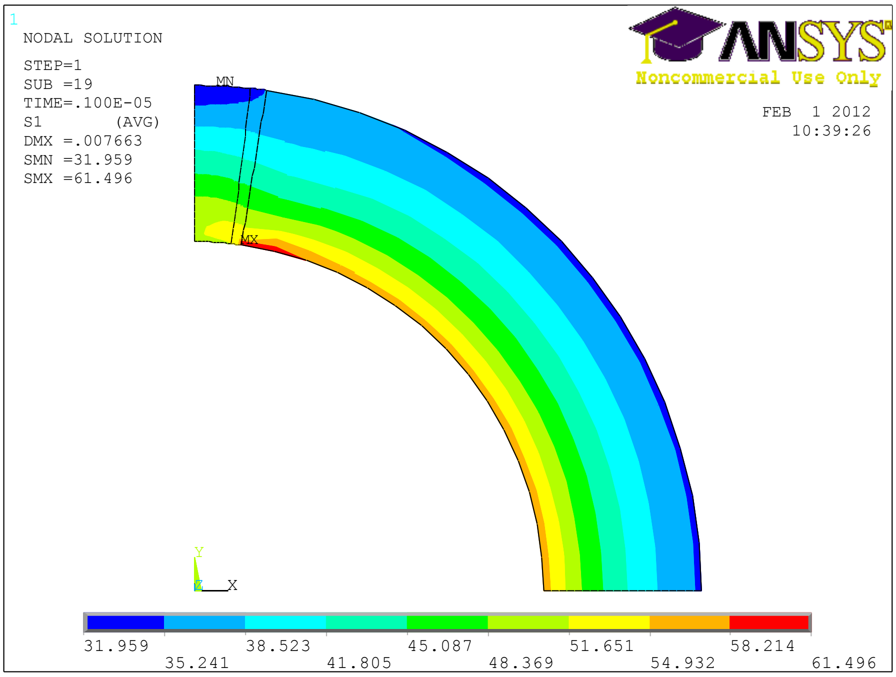

↑ Fig. 5.2.1a 1st principal stress immediately after the simulation started

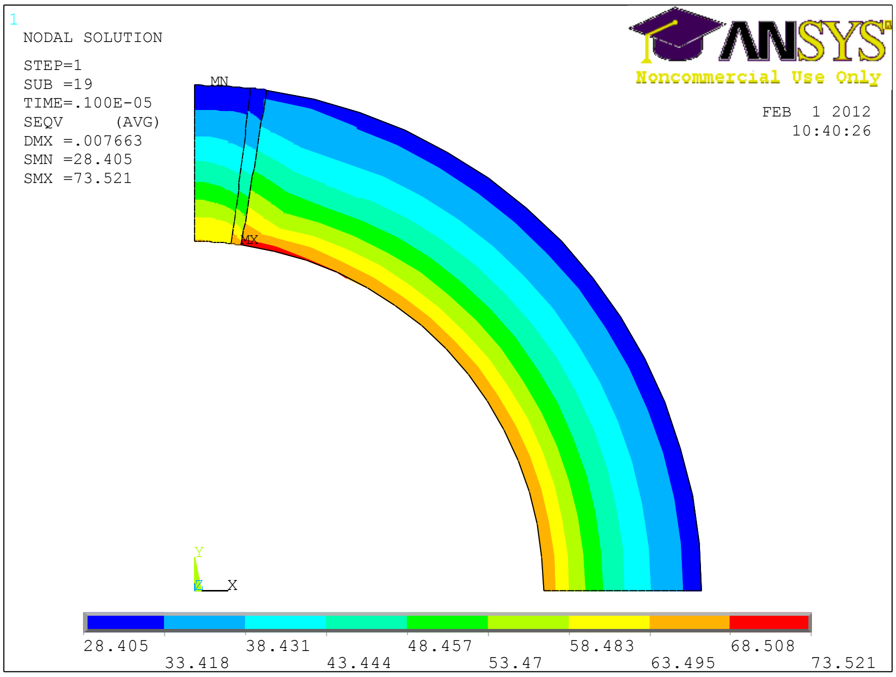

↑ Fig. 5.2.1b Mises stress immediately after the simulation started

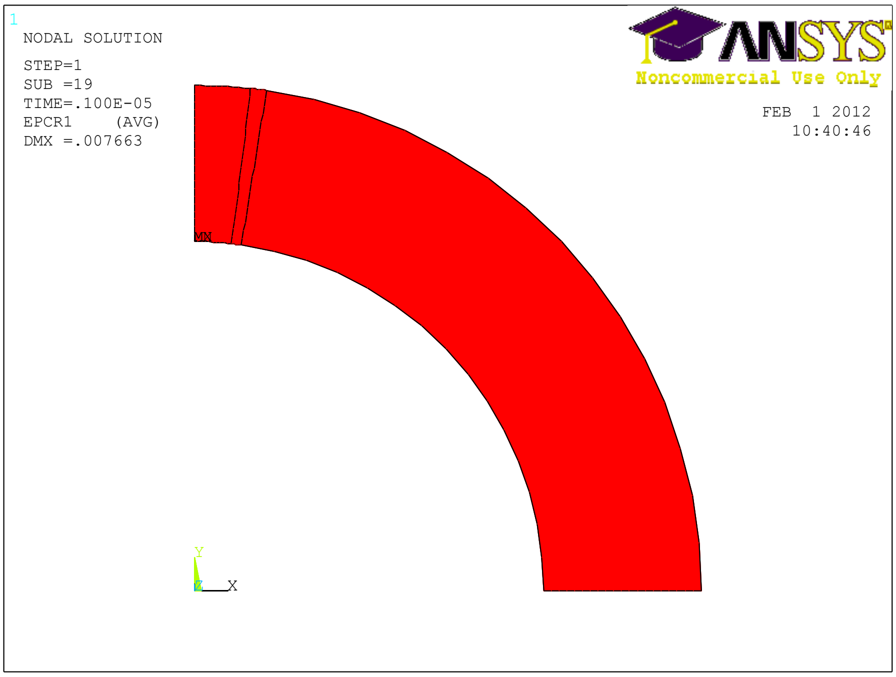

↑ Fig. 5.2.1c creep strain immediately after the simulation started

5.2.2 50 hours after pressured

After 50 hours out of 6700 hours of simulation, we can see drastic changes in stress distribution in all 1st, 2nd, and 3rd principal stress distributions. The concentration of stresses prominently shift from inner surface to outer surface, and heat affected zone close to the outer surface holds the highest stress value (fig.5.2.2a, fig. 5.2.2b, fig. 5.2.2c). On the contrary, von Mises stress plummets greatly in heat affected zone in fig. 5.2.2d. For creep strain distribution in fig. 5.2.2e, creep strain is highest near the inner surface of the material.

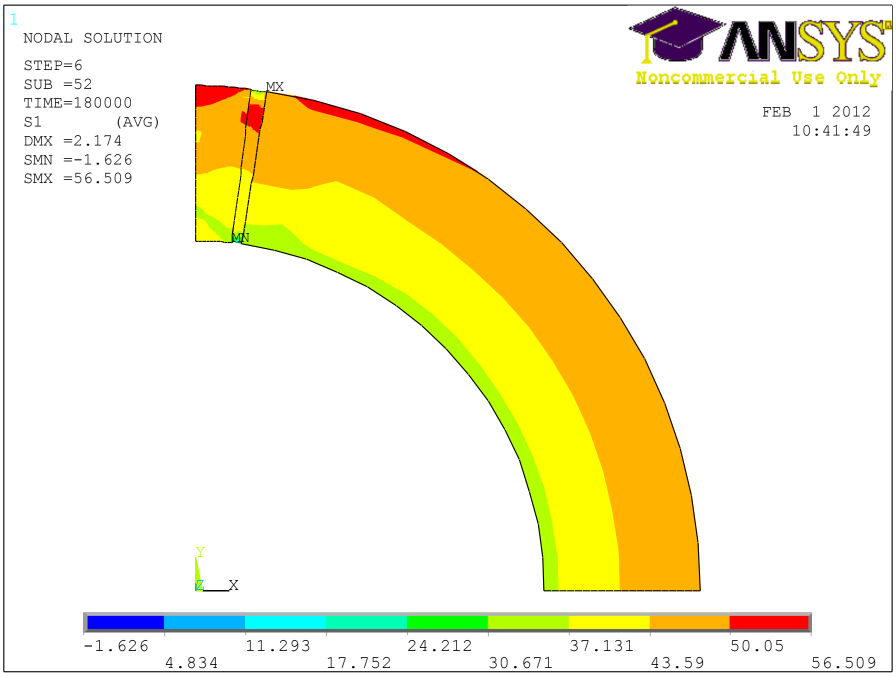

↑ Fig. 5.2.2a 1st principal stress 50 hours later

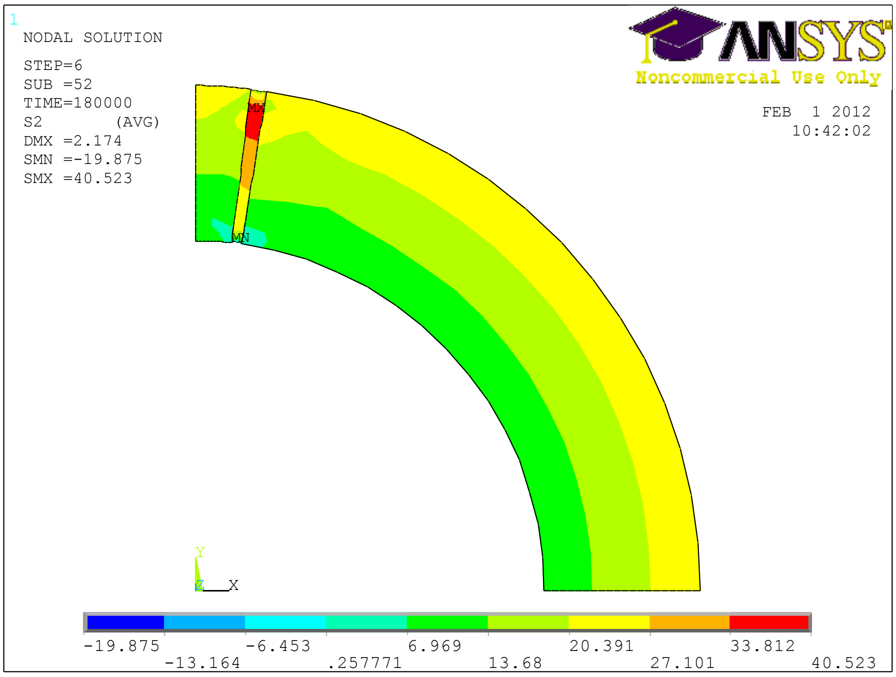

↑ Fig. 5.2.2b 2ndprincipal stress 50 hours later

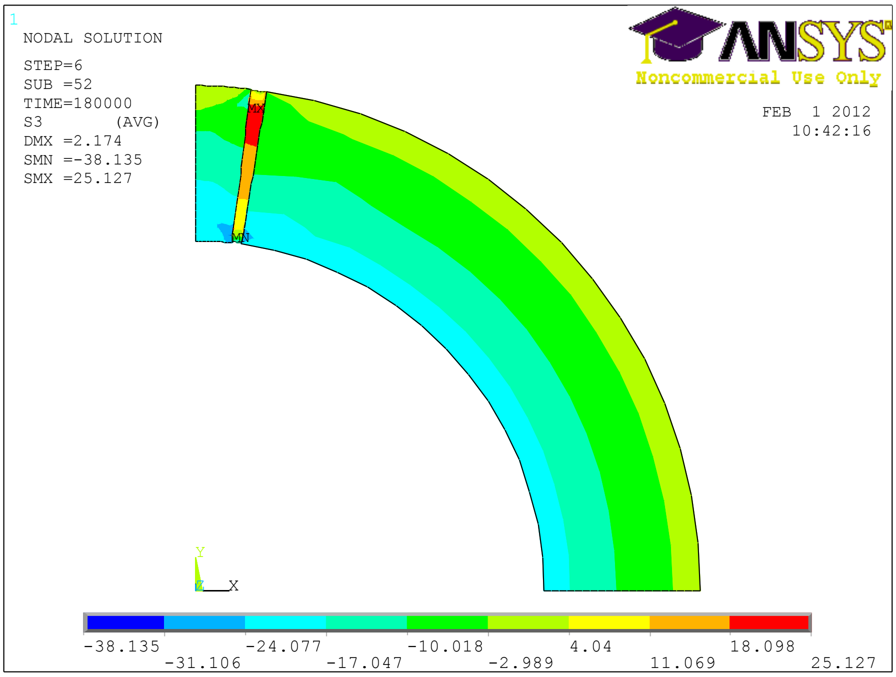

↑ Fig. 5.2.2c 3rd principal stress 50 hours later

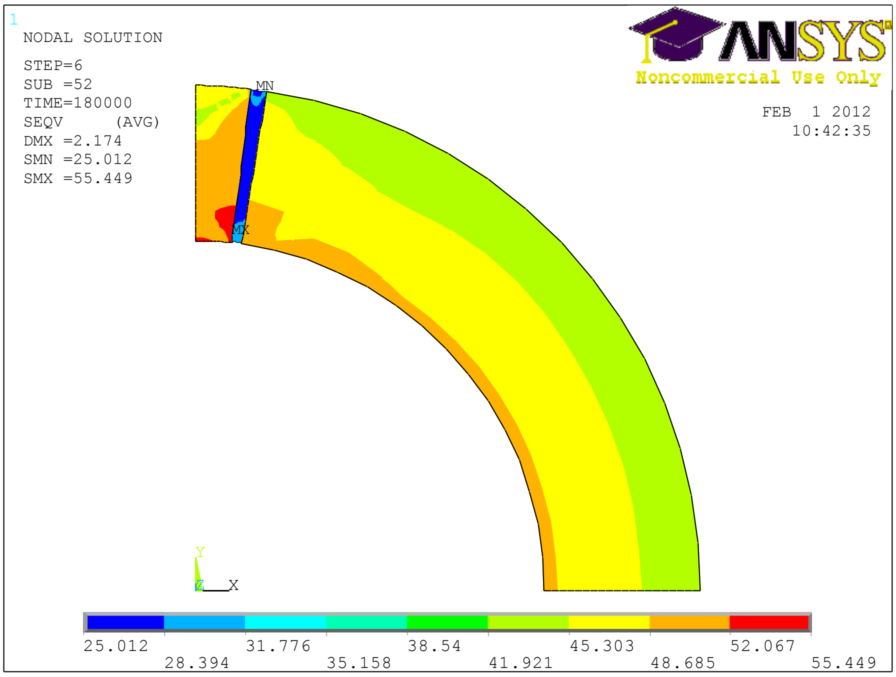

↑ Fig. 5.2.2d von Mises stress 50 hours later

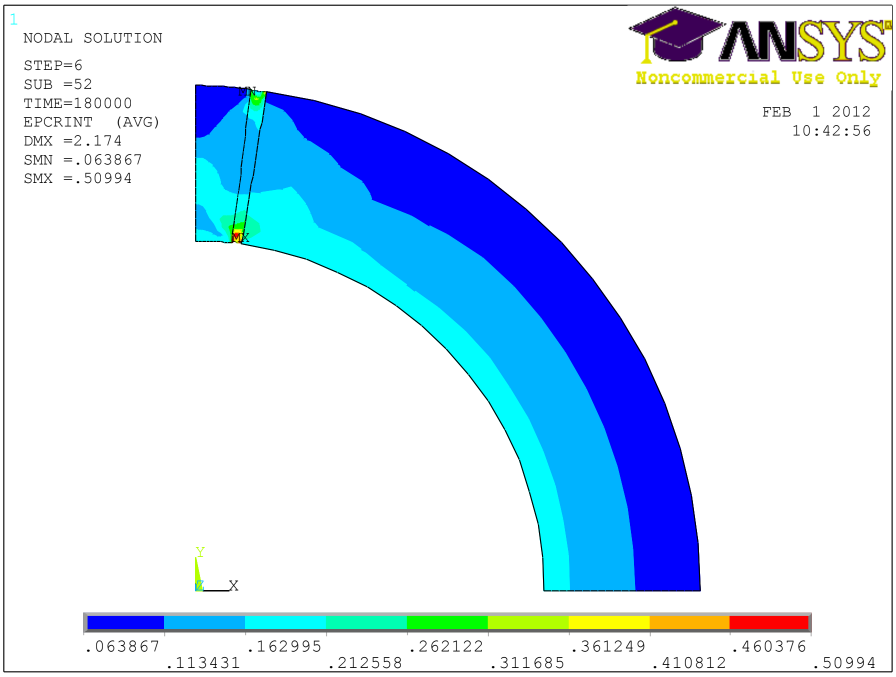

↑ Fig. 5.2.2f creep strain rate 50 hours later

5.2.3 6700 hours after pressured

Again, after more than 6000 hours passed, stress distributions radically change; however, the tendency is still the same with higher stress value on the outer surface of the material. Anyhow, we also found that there is a very high stress peaks located between heat affected zone and weld metal with highest value of 94.563 MPa in 1st principal stress, 78.514 MPa in 2nd principal stress, and 63.165 MPa in 3rd principal stress. The cause is thought to be the drastic difference in Norton's creep constants in the areas, hence after long period of time, creep strain grows large and the interval between two areas is affected most.

Triaxiality factor is calculated here and the result is showed as a contour graph in fig. 5.2.3e. The result is as expected and fit considerably well with creep void density distribution in fig. 5.1.2a.

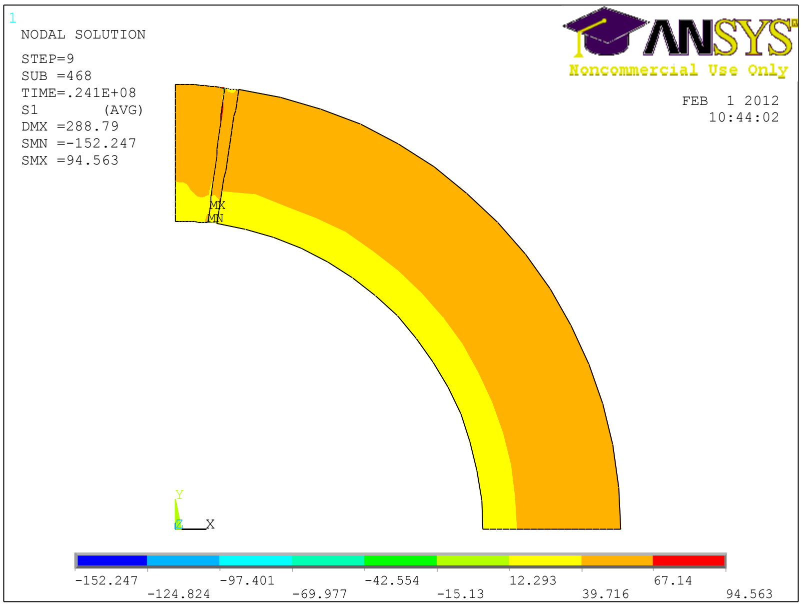

↑ Fig. 5.2.3a 1st principal stress 6700 hours later

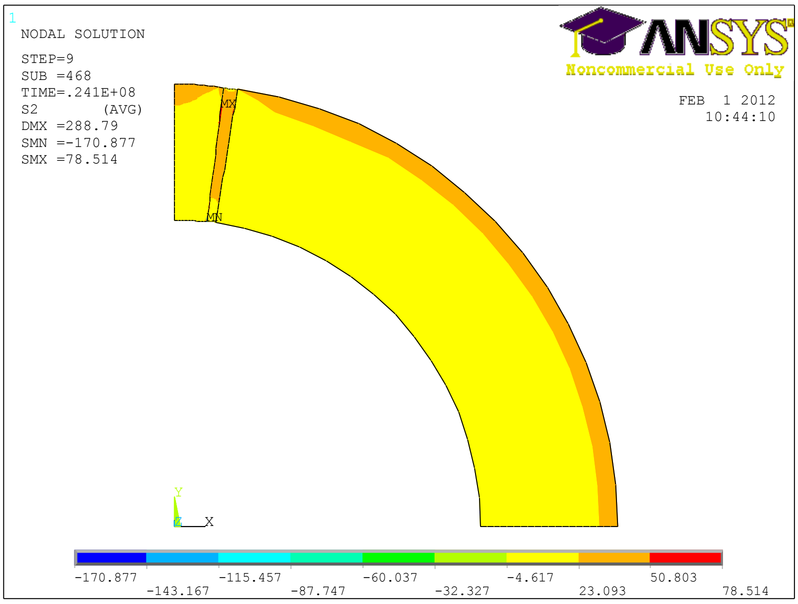

↑ Fig. 5.2.3b 2ndprincipal stress 6700 hours later

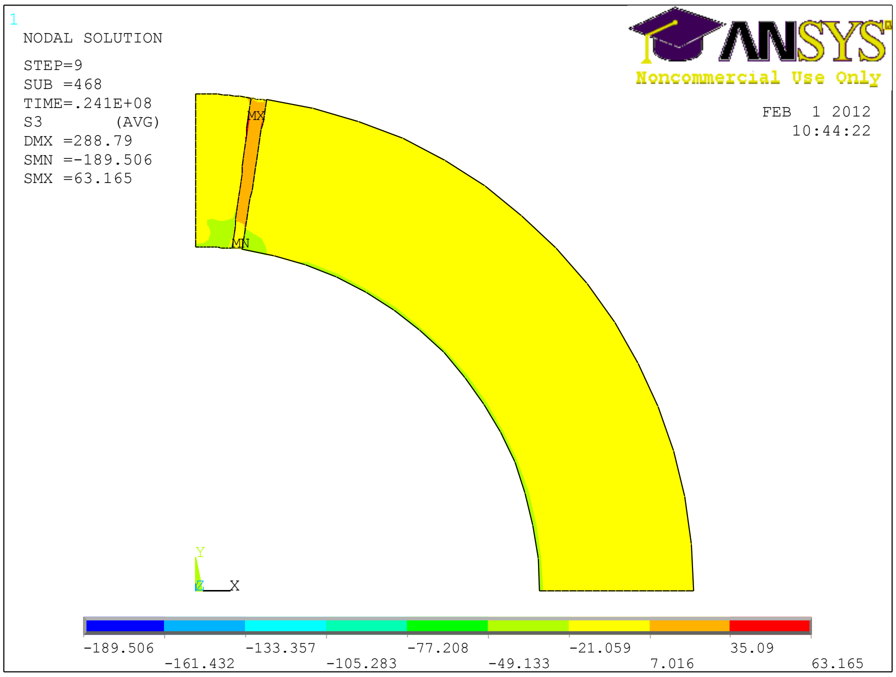

↑ Fig. 5.2.3c 3rd principal stress 6700 hours later

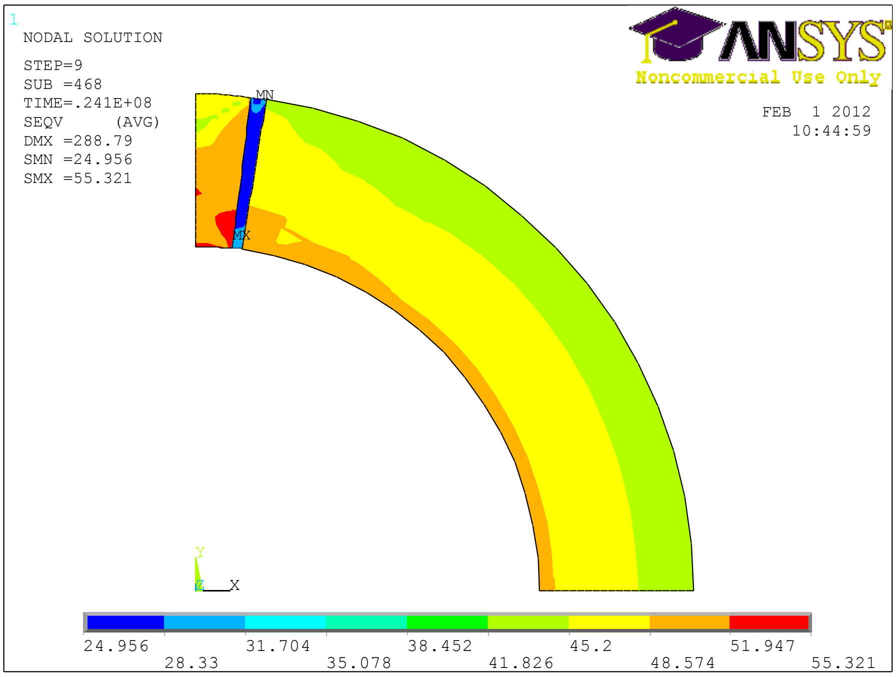

↑ Fig. 5.2.3d von Mises stress 6700 hours later

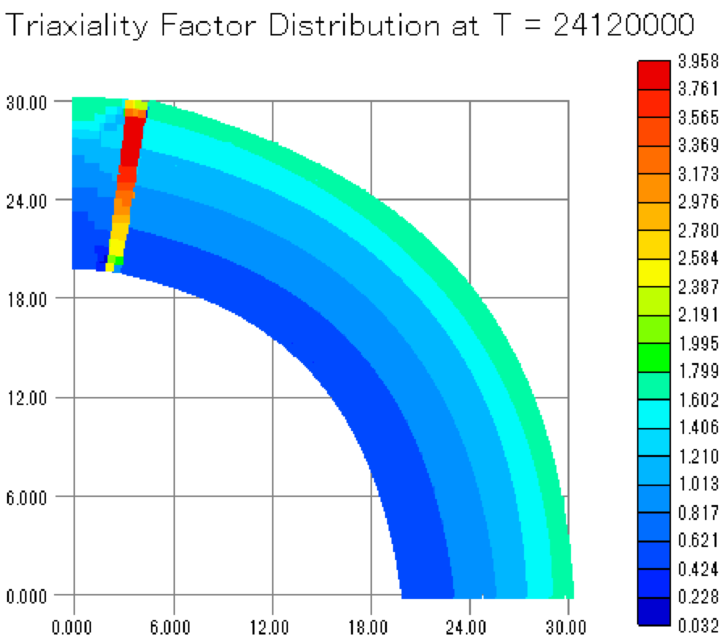

↑ Fig. 5.2.3e triaxiality factor 6700 hours later

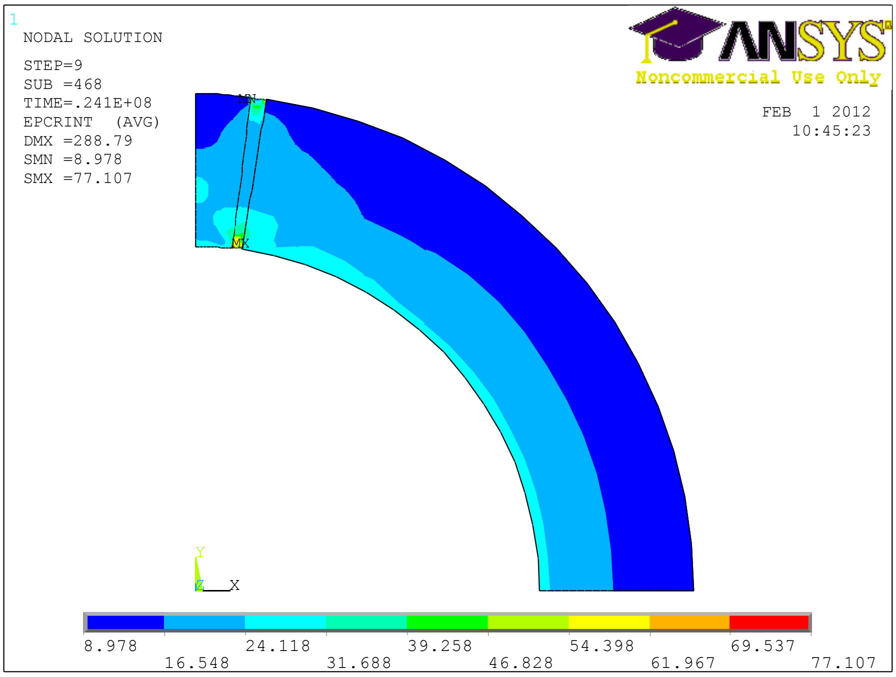

↑ Fig. 5.2.3f creep strain distribution 6700 hours later

Chapter 6: Conclusion and Plans for Further Research

It is accepted that there are many restrictions on both time and knowledge that make this research not as perfect as it could be; however, we hope that at least it would open a new perspective, a new approach to tackle type IV crack problem in USC power plants. Here are the discussions and ideas of how this research topic could be improved.

1.) From the result, it is undoubtedly clear that creep void density distribution is significantly correlated with creep void area ratio distribution; even though, there are some observation areas (particularly the near the outer surface of column 16-17 in weld metal area) where, although with small amount of creep voids, have very high creep area ratio and some other areas vice versa. Fig. 6.1 below showed the areas of creep void distribution and creep void area ratio where disputes were located.

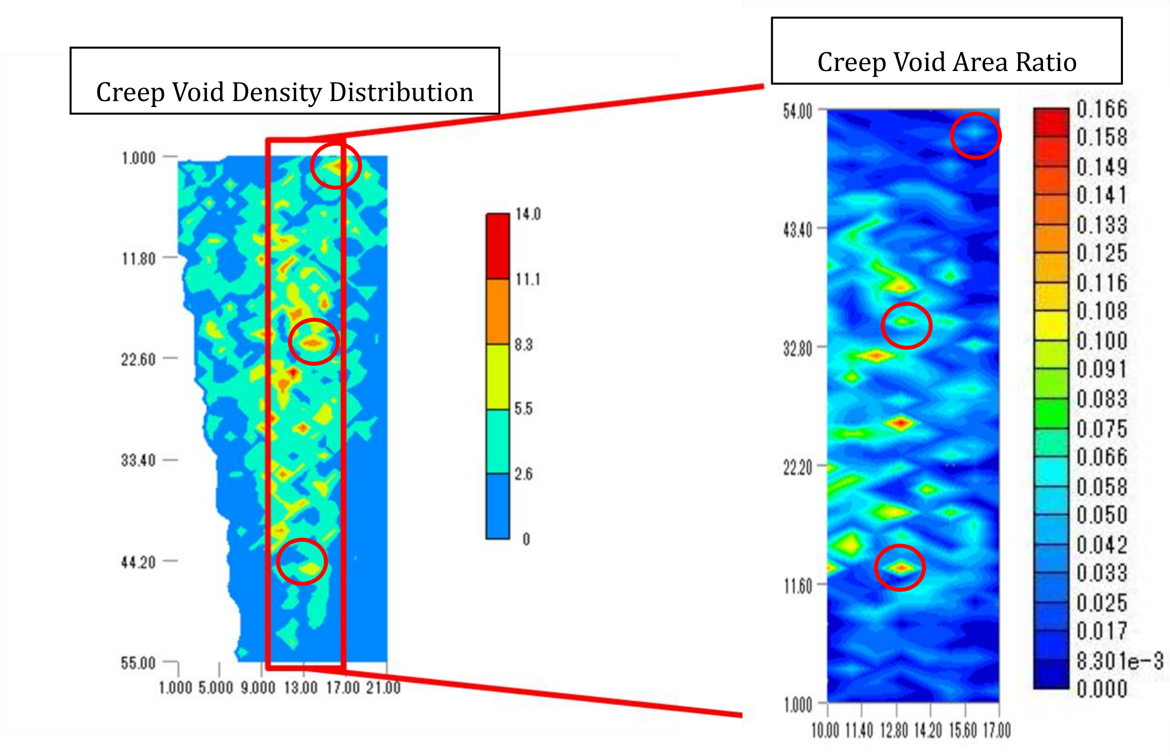

↑ Fig. 6.1 disputes between creep void distribution and creep void area ratio

It has always been an argument whether creep void density distribution or creep void area ratio distribution should be considered priority in creep damage evaluation. Of course, the simpler method, creep void density distribution, is more popular, yet it is inadequate to admit creep void density distribution as a better criterion.

Here with the data on triaxiality factor, grain type boundary, and Vickers hardness, it is clear that the scope of fine grain area fit better in creep void density distribution. So, we would conclude that creep area ratio method not only takes unnecessary effort but also provides inferior result to conventional creep void density distribution method.

In addition, the creep void density distribution is noticeably coarse. This is the result of one SEM photograph per one creep void measurement which can be easily improved by increasing observation planes from the source we had. By using image processing software to stitch those photographs together and recreate new photos in the interval between the centers of two adjacent photos, we can augment the observation nodes by almost twice in number. This process would definitely help smoothen the contour graph as well as the line chart.

2.) On the contrary, the statistical data of creep void distribution in graph 5.1.2a and creep void area ratio in graph 5.1.2c showed a very similar direction (those two graphs are being showed below). Most peaks were located in the same distance from inner surface; however, sample space of creep void distribution was somewhat wider. The fewer of number of SEM photographs left the line chart of creep void area ratio with higher standard deviation value。 Despite the difference in number of sample space both graphs showed the very similar trend.

3.) In vertical axis analysis, the results of creep void distribution and creep void area ratio were showed in graph 5.1.2b and 5.1.2d. The highest average values of the data were evidentially on different position. Creep void distribution was highest in column 12th and 15th, while in creep area ratio the highest values were in column 10th and 13th and fell drastically in column 11th and 13th. Overall tendencies were considerably similar, high on the left end to the center, and then gradually decline the more right we proceeded.

4.) We found a strong relationship between grain type boundary and Vickers hardness. Considering fig. 5.1.3b, the grain type boundary mask we mapped onto Vickers hardness contour graph fit almost perfectly with the pattern of stripes of surface hardness. Thus, we could not deny that there was a relation between grain type and Vickers hardness. Here, we would like to propose two hypothesis statements on the relationship.

Firstly, there might be a change in micro structure of fine grain area during the welding process, and it resulted in a plummet of the area's hardness. The new and softer characteristic consequently weakened the area's creep strength. And this was how creep voids tended to concentrate solely in the fine grain area.

Secondly, it was not because of the change in micro structure of the area, but the difference in properties especially hardness of weld metal and base metal that made the area in between suffer high stress. In addition to the excessive stress concentration, high temperature and high pressure also foster the gradual weakening in the interval between base metal and weld metal.

To verify whether which of the hypothesis statement was true, if any, we needed to conduct another observation of the welded material which had yet been experimented. The further observation result would help explain what actually happened with fine grain area. If the result shows that fine grain has the same or higher Vickers hardness than base metal, then the second hypothesis statement is true. Otherwise, it can be stated that the first hypothesis is true and the degradation of fine grain area happened during welding procedure.

5.) After 6700 hours of finite element simulation, the results of principal stresses and von Mises stress were taken to calculate triaxiality factor which is showned below in fig. 5.2.1e. Triaxiality factor is highest in the center of heat affected zone, which is where most creep voids were located. While HAZ closer to inner surface has much less triaxiality factor value, outer surface holds considerably high figure. Even this characteristic supports the observation result. This shows great relation between creep void rupture and triaxiality factor. However, we also simulated three-dimension simulation but it has not been accomplished yet. Although, the results were supposed to be the same, it is still important to check the simulating condition that is closest to real experiment.

Acknowledgement

"There is joy in work. There is no happiness except in the realization that we have accomplished something."

-Henry Ford

A blind man as I was the first moment I enter Sakai・Izumi Lab, I was exceedingly uncertain about what research theme and area I would engage in. This research would have never existed from the beginning if it were not for my supervisor, associated professor, Satoshi Izumi, who not only gave me whole new visions of what could be accomplished as a researcher but also reserved my morale high when I confronted daunting challenges. His austerity gradually polished me into a much more efficient individual as well.

Next, I place on record, my sincere gratitude to my professor, Shinsuke Sakai, whose expertise, connection and interest concerning creep rupture significantly help contribute to my research. His passion in the issue implicitly drove me to perform my very best to perfect the result.

The most important person with whom I spent most of the research time and answered to every of my annoying trivial questions could have been no one else but Mr. Kenta Yamagiwa, who currently works at National Institute of Occupational Safety and Health. All the measuring instruments including scanning electron microscope, micro Vickers hardness measuring instrument and surface polisher are all sponsored by National Institute of Occupational Safety and Health. Constant conversations with him intensify my urge to pay Utah a visit and enjoy its beautiful nature and culture.

I also take this opportunity to express my gratitude toward Central Research Institute of Electric Power Industry for the test specimen and all the heavy workload of conditioning before transferring mod.9Cr steel specimen to me, and for the opportunity to have fascinating discussions with experts in the area concerning creep void characteristics.

I always feel blessed to be a part of my vivacious research lab with considerate seniors and outlandish classmates (labfellows). The list starts with omniscience Maeda sempai, who offered very kind advice over my former title, an American-series-addict Matsumoto sempai, who shares a lot of interest with me in addition to babysit me all the time when we were conducting experiments at National Institute of Occupational Safety and Health. Next, Ogata sempai, Kamiya sempai and Morizumi sempai, who expert at finite element analysis software and supervised me through the whole FEM analysis section. Son sempai and Kyoku sempai, who share the same ryugakusei fate with me at Sakai・Izumi Lab and periodically helped make my lunch time much more enjoyable. Muranaka sempai, who always hosts lab sport events and let me burn my fat every once in a while. And thank to every other seniors as well for this wonderful 1-year time.

I am indebted to many of my colleagues who are all worth mentioned. Narita, the friend in Tokyo University who I have known for the longest, thank you for saving my life many times and for countless unambiguous advices all through these years. To Koshiishi, the labfellow whose 70% of research area is identical to mine. We have been mutually scratching each other's back for the last six months. Many thanks to Shirai, lab's soccer king with great sense of humor, to Ikeda, our trip and party planner, to Kobayashi, master body-builder, and to Kuriyama, South African Japanese. Everyone made my year an unforgettable memory; I am truly gretful.

Lastly, it is an honor for me to give special thanks to my parents who set education as first priority, and thus helped me come this far, to my sweet sisters and two petit nieces who help me feel grown up and constantly urge me to strive harder, to my Sendagian friends who pull me back to sanity every time I am about to go crazy, to Pang who help soothe my pain and keep me smiling.

Watcharaphon Uttranuson

February 2nd, 2012

References

[1] Tetsushi Kataoka, Shinsuke Sakai, Cr-Mo-V 鋼のクリープ損傷過程におけるボイドの３次元形態および空間分布の変化, university of Tokyo, 2010.

[2] Takashi Ogata, Takayuki Sakai, Masatsugu Yaguchi, Clarification of damage condition and development of damage evaluation method of a mod.9Ce-1Mo steel longitudinal welded tube under internal pressure creep, p.2-3, 10-12, Central Research Institute of Electric Power Industry, Q07002, 2008.

[3] Kenichi Yatsuda, Shinsuke Sakai, 溶接鋼管エルボの溶接部形状とクリープ損傷度との関係, university of Tokyo, 2006.

[4] Hitachi Group, Supercritical pressure coal-fired thermal power plant, Hitachi Ltd, 2012.

[5] IEA, Energy Balances of OECD and Non-OECD countries, 2004.

[6] Bob McIlvaine, Power air quality insights, McIlvaine Company, April, 2011

[7] Jay Kilburn, Handling Nine-chrome steel in HRSGs, Power Engineering Magazine, February, 2006.

[8] Takayuki Sakai, Matatsugu Yaguchi, Takashi Ogata, Development of damage assessment system for weld joints based on stress analysis for boiler tube, p.11-14, Central Research Institute of Electric Power Industry, Q09005, May, 2010.

[10] Alberto Jose Pego Fernandez, Mechanical properties of hybrid laser-MIG welding and spot welding on lab joint, p. 23-24, Lulea University of Technology, 2008.

[11] Dr. Rainer Quinkertz, Andreas Ulma, Edwin Gobercht, Michael Wechsung, USC Steam Turbine technology for maximum efficiency and operational flexibility, Siemens AG 2008, p.3-5.

[12] G. Maresca, P.P. Milella, G. Pino, A critical review of triaxiality based failure criteria, IGF 13-Cassino 27 e 28 Maggio, 1997.

[13] Josef Betten, Creep Mechanics 3rd edition Springer, p. 49-63, 2008.

[14] The National Institute of Standards and Technology, Creep and Constitutive Models for Near-Eutectic SnPb , U.S. Commerce Department